Journal of Computational Physics 469 (2022) 111357

Contents lists available at ScienceDirect

Journal of Computational Physics

www.elsevier.com/locate/jcp

Conservative integrators for vortex blob methods on the plane

Cem Gormezano [a,*], Jean-Christophe Nave [b], Andy T.S. Wan [c]

[a] Mathematical Institute, University of Oxford, Oxford, OX2 6GG, UK
[b] Department of Mathematics and Statistics, McGill University, Montréal, QC, H3A 0B9, Canada
[c] Department of Mathematics and Statistics, University of Northern British Columbia, Prince George, BC, V2N 4Z9, Canada

ARTICLE INFO

Article history:
Received 13 November 2021
Received in revised form 15 May 2022
Accepted 29 May 2022
Available online 8 July 2022

Keywords:
Dynamical systems
Fluid dynamics
Vortex method
Conservative methods
Discrete Multiplier Method
Long-term integration

ABSTRACT

Conservative integrators have recently been derived for many-body systems using the Discrete Multiplier Method, specifically for the point vortex problems in [1]. In the present paper, we extend this work to derive conservative symmetric second-order one-step integrators for a family of vortex blob models. A rational function approximation was used to approximate the exponential integral which appears in the Hamiltonian. Conservative properties and second order convergence are proved. Numerical experiments are shown to verify the conservative property of these integrators, their second-order accuracy, and as well as the resulting spatial and temporal accuracy of the vortex blob method. Moreover, the derived implicit conservative integrators are shown to better preserve conserved quantities than standard higher-order explicit integrators on comparable computation times.

1. Introduction

In recent years, structure preservation has become an important property to consider when devising numerical methods for differential equations. The main idea is to design discretizations which preserve important underlying structures of the continuous problem at the discrete level. For ordinary differential equations (ODEs), geometric integrators, such as energy-momentum method [2,3], symplectic integrators [4,5], variational integrators [6], Lie group methods [7,8], and the method of invariantization [9–11] are examples of discretizations which can preserve symplectic structure, first integrals, phase space volume, or symmetries at the discrete level. Conservative integrators are structure-preserving numerical schemes which preserve the first integrals, invariants, or equivalently, conserved quantities of the ODEs up to machine precision. One main motivation behind such integrators is their intrinsic long-term stability properties [12] making them favorable in the long-term study of dynamical systems, such as in population dynamics, celestial mechanics, molecular dynamics, and fluid mechanics [1].

The purpose of this paper is to present conservative integrators for the higher-order vortex methods introduced by [13] for the inviscid, incompressible Euler's equations in the plane. Vortex methods are a class of numerical methods that approximates the vorticity field associated with the solution of the inviscid, incompressible Euler equations. In contrast to point vortex method [14] where the vorticity field is approximated by a finite number of Dirac distributions, vortex blob methods regularize the Dirac distributions with a finite superposition of smooth localized vorticity fields, referred to as

* Corresponding author.
E-mail addresses: cem.gormezano@maths.ox.ac.uk, cem.gormezano@mail.mcgill.ca (C. Gormezano), jcnave@math.mcgill.ca (J.-C. Nave), andy.wan@unbc.ca (A.T.S. Wan).

https://doi.org/10.1016/j.jcp.2022.111357
0021-9991/

vortex blobs. The resulting vorticity field associated with each vortex resembles a smooth blob with a width δ that scales with the size of the discretization. As δ tends to zero, these blobs converge to the Dirac distribution and one recovers the exact solution to the invicid, incompressible Euler's equations in the plane [15]. For invicid, incompressible flows, Hald [16] showed that as the number of vortices increases for a special class of blob functions, solution of the vortex methods converges to the solution of Euler's equations with second order accuracy for an arbitrarily long time interval. Later, Beale and Majda [17,18] showed that vortex methods could be chosen so that they converge with higher-order accuracy. Moreover, in [13], Beale and Majda obtained higher-order vortex methods in two and three dimensions through superposition of vorticity fields involving Gaussians with different scalings and products of even polynomials with Gaussians. Vortex methods have found applications in many fields from computational aerodynamics [19–21] to combustion [22,23]. A brief survey of different vortex methods in the literature can be found in [24]. Also, a more recent vortex method based on a new singular vortex theory for regularized Euler fluid equations of ideal incompressible flow in the plane can be found in [25].

In essence, vortex methods lead to a system of ordinary differential equations (ODEs), known as the vortex blob equations, describing the evolution of interacting vortices approximating the vorticity field. Traditionally, standard integrators are used to obtain numerical solutions to the vortex blob equations, such as Runge-Kutta methods in [13]. In contrast, we construct conservative integrators for this ODEs using the Discrete Multiplier Method (DMM) introduced by Wan et al. in [26]. The main idea of DMM is to discretize the so-called characteristics [27] and conservation law multipliers [28] for ODEs so that the discrete multiplier conditions hold. In [1], such framework was used to derive conservative integrators for various many-body systems, including n-species Lotka–Volterra system, the n-body problem with radially symmetric potential, and the n-point vortex models on the plane and the unit sphere. In this paper, we will extend the results on the planar point vortex method of [1] by deriving conservative integrators for planar vortex blob methods. We believe that this is a natural first extension of DMM, even though such vortex blob model had previously been shown to be deficient when compared to the Euler-alpha model in certain scenarios [29].

This paper is organized as follows. In Section 1, we briefly review the higher-order vortex methods given in [13] and introduce some common notations used throughout the paper. In Section 2, we introduce additional notations and conventions used throughout the paper, along with a quick review of DMM. Specifically, we state differential relations between conserved quantities and conservation law multipliers, and the discretized versions in order to construct a conservative integrator. Moreover, we review a known result regarding symmetric schemes having even order of accuracy. In Section 3, we derive conservative discretizations for the vortex blob equations with 2$^{\text{nd}}$, 4$^{\text{th}}$, and 6$^{\text{th}}$ order velocity kernels. Section 4 is then devoted to numerical results. First, we verify that the DMM-based conservative integrators preserve all the conserved quantities up to machine precision, in contrast to standard integrators such as the implicit midpoint method, Ralston's second-order method, and Ralston's fourth-order method. Second, we demonstrate that the conservative schemes yield conserved quantities of vortex blob equations that converge to the original conserved integrals of Euler's equations, as the number of vortices increases. Third, we illustrate that the long-term vortex trajectories from the conservative schemes are qualitatively closer to the exact trajectories than standard integrators. We then show numerically that the conservative integrators are second-order accurate in time and verify that the vortex blob method using the conservative integrator converges to the theoretical orders previously reported by Beale and Majda using Runge-Kutta integrators. Lastly, we compare computation times of the conservative integrators versus standard integrators and show that the derived schemes are better at preserving conserved quantities on comparable computation times. Finally, in the Section 5, we give several concluding remarks and discuss interesting avenues for further exploration.

1.1. Brief review of the vortex blob method

In this subsection, we review the derivation of the vortex blob model and its associated conserved quantities, along with introducing common notations which will be used throughout this paper. Readers familiar with this background may skip to the next section.

In the absence of body forces, the planar inviscid, incompressible Euler's equations for a fluid with constant density ρ are given by,

$$\begin{aligned}\frac{\partial \boldsymbol{v}}{\partial t}+\boldsymbol{v}\cdot\nabla\boldsymbol{v}&=-\frac{1}{\rho}\nabla P,\\ \nabla\cdot\boldsymbol{v}&=0,\end{aligned} \tag{1}$$

where $\boldsymbol{v}(\boldsymbol{z},t)$ denotes the velocity vector field and $P(\boldsymbol{z},t)$ denotes the scalar pressure field of the fluid at a point $\boldsymbol{z}=[x,\ y]^T$ and time t. Recalling the vorticity is the scalar field $\omega(\boldsymbol{z},t)$ satisfying $\omega\hat{\boldsymbol{k}}=\nabla\times\boldsymbol{v}$, applying the curl on both sides of (1) yields the vorticity equation [30],

$$\frac{D\omega}{Dt}=\frac{\partial\omega}{\partial t}+\boldsymbol{v}\cdot\nabla\omega=0. \tag{2}$$

Equation (2) implies that, in the Lagrangian description of the fluid, the vorticity of a fluid particle is conserved along its trajectory. The problem we wish to solve is the vorticity-velocity formulation given by,

$$\frac{D\omega}{Dt} = 0, \tag{3a}$$

$$\omega(\boldsymbol{z}, 0) = \omega_0 \quad \text{on} \quad \Omega_0, \tag{3b}$$

$$\nabla \cdot \boldsymbol{v} = 0, \tag{3c}$$

$$\nabla \times \boldsymbol{v} = \omega, \tag{3d}$$

$$\|\boldsymbol{v}(\boldsymbol{z}, t)\|_2 \to 0 \quad \text{as} \quad \|\boldsymbol{z}\|_2 \to \infty, \tag{3e}$$

where ω_0 is assumed to be compactly supported on Ω_0. Equations (3c)–(3e) can be combined to give the velocity in terms of vorticity through the Biot-Savart law yielding,

$$\boldsymbol{v}(\boldsymbol{z}, t) = \iint\limits_{\Omega(t)} \boldsymbol{K}\left(\boldsymbol{z} - \boldsymbol{z}'\right) \omega\left(\boldsymbol{z}', t\right)\, d\boldsymbol{z}'. \tag{4}$$

Here $\boldsymbol{K}(\boldsymbol{z}) = \frac{1}{2\pi\|\boldsymbol{z}\|_2^2}[-y, x]^T$ is the velocity kernel [30] and $\Omega(t)$ is the domain with non-zero ω at time t. Thus, the problem posed by (3a)–(3e) reduces to (3a), (3b), and (4) and it follows from equations (3a)–(3e) that the following integrals are conserved for all time [31] (Chapter 7 of Section 7.3):

1. The total vorticity in $\Omega(t)$, or in other words the circulation around $\partial\Omega(t)$, given by,

$$\Gamma := \Gamma[\omega](t) = \iint\limits_{\Omega(t)} \omega(\boldsymbol{z}, t)\, d\boldsymbol{z}. \tag{5}$$

2. The x and y components of the total fluid impulse (or momentum) that must be applied to the fluid in $\Omega(t)$ to generate the motion governed by the stream function $\Phi(\boldsymbol{z}, t)$ from rest, where $\Phi(\boldsymbol{z}, t) := \Psi(\boldsymbol{z}, t) + \frac{\Gamma}{2\pi}\log\|\boldsymbol{z}\|_2$ with $\nabla \times (\Psi\hat{\boldsymbol{k}}) = \boldsymbol{v}$. These components are,

$$\mathcal{P}_x := \mathcal{P}_x[\omega](t) = \rho \iint\limits_{\Omega(t)} y\omega(\boldsymbol{z}, t)\, d\boldsymbol{z}, \qquad \mathcal{P}_y := \mathcal{P}_y[\omega](t) = -\rho \iint\limits_{\Omega(t)} x\omega(\boldsymbol{z}, t)\, d\boldsymbol{z}. \tag{6}$$

3. The total moment (or angular momentum) about the origin of the force impulse required to generate the motion determined by $\Phi(\boldsymbol{z}, t)$ in $\Omega(t)$, which is given by,

$$\mathcal{L} := \mathcal{L}[\omega](t) = -\frac{\rho}{2} \iint\limits_{\Omega(t)} \|\boldsymbol{z}\|_2^2\, \omega(\boldsymbol{z}, t)\, d\boldsymbol{z}. \tag{7}$$

4. The kinetic energy of the fluid associated with the fixed amount of total vorticity being distributed given by,

$$\mathcal{H} := \mathcal{H}[\omega](t) = -\frac{\rho}{8\pi} \iint\limits_{\Omega(t)'} \iint\limits_{\Omega(t)} \omega(\boldsymbol{z}, t)\, \omega\left(\boldsymbol{z}', t\right) \log\|\boldsymbol{z} - \boldsymbol{z}'\|_2^2\, d\boldsymbol{z}\, d\boldsymbol{z}'. \tag{8}$$

Vortex methods arise from approximating the vorticity field ω via a system of ODEs as follows. First, the domain Ω_0 is discretized using a uniform square grid of size h and point vortices are introduced at the center of each h by h square cell so that the i-th vortex initially has vorticity $\omega_0(\boldsymbol{z}_i^h(0))$, where $\boldsymbol{z}_i^h(t)$ is the position of the i-th vortex at time t and its vorticity remains constant by equation (3a). Moreover, equation (5) implies that $\Omega(t)$ contains the same vortices as Ω_0 for all time. Thus, we can directly discretize (4) to formulate ODEs describing the trajectories of M vortices contained in $\Omega(t)$,

$$\dot{\boldsymbol{z}}_i^h = \sum_{\substack{j=1 \\ j \neq i}}^{M} \boldsymbol{K}\left(\boldsymbol{z}_i^h - \boldsymbol{z}_j^h\right) \omega_j h^2, \quad \boldsymbol{z}_i^h(0) = [i_1 h,\ i_2 h], \quad i \in \{1 \ldots M\}, \quad i_1, i_2 \in \mathbb{Z}, \tag{9}$$

where we denoted $\omega_i = \omega_0(\boldsymbol{z}_i^h(0))$ and velocity field $\boldsymbol{v}$ can be approximated by $\boldsymbol{v}^h$,

$$\boldsymbol{v}^h(\boldsymbol{z}, t) = \sum_{j=1}^{M} \boldsymbol{K}\left(\boldsymbol{z} - \boldsymbol{z}_j^h(t)\right) \omega_j h^2. \tag{10}$$

It can be observed that $\boldsymbol{K}(\boldsymbol{z}_i^h - \boldsymbol{z}_j^h)$ becomes singular as two vortices approach each other. At this stage the approximate vorticity field associated with (10) leads to the *point vortex method*. Since $\boldsymbol{K}$ is singular at $\boldsymbol{z}_i^h = \boldsymbol{z}_j^h$, it can be regularized by a mollification $\boldsymbol{K}^{\delta}$. The choice of mollification determines the accuracy of the vortex method and in [13], Beale and Majda chose the family of kernels,

$$\boldsymbol{K}^{\delta,(m)}(\boldsymbol{z})=\frac{[-y,x]^T}{2\pi\,\|\boldsymbol{z}\|_2^2}\left[1-Q^{(m)}\left(\frac{\|\boldsymbol{z}\|_2^2}{\delta^2}\right)\exp\left(-\frac{\|\boldsymbol{z}\|_2^2}{\delta^2}\right)\right]. \tag{11}$$

Here δ is a smoothing parameter, m denotes the order of the vortex method, and $Q^{(m)}(r)$ is the $\frac{m}{2}-1$ order Laguerre polynomial normalized with unit constant term:

$$Q^{(2)}(r)=1,\quad Q^{(4)}(r)=1-r,\quad Q^{(6)}(r)=1-2r+\frac{r^2}{2}\ \ldots$$

With mollification, the approximate vorticity field associated with $\boldsymbol{v}^h$ corresponds to a linear combination of localized vortex densities resembling smooth "blobs", leading to the *vortex blob method* given by (9) with $\boldsymbol{K}^{\delta,(m)}$. For the family of mollified kernels of equation (11), the approximate vorticity field associated with $\boldsymbol{v}^h$ is given by,

$$\omega^h(\boldsymbol{z},t)=\sum_{i=1}^{M}\omega_i h^2\zeta^{\delta,(m)}\left(\boldsymbol{z}-\boldsymbol{z}_i^h(t)\right), \tag{12}$$

where $\zeta^{\delta,(m)}(\boldsymbol{z})=P^{(m/2)}\left(\|\boldsymbol{z}\|_2^2/\delta^2\right)\exp\left(\|\boldsymbol{z}\|_2^2/\delta^2\right)/\delta^2$, with the first few orders of $P^{(m/2)}(\cdot)$ given by,

$$P^{(1)}(r)=\frac{1}{\pi},\qquad P^{(2)}(r)=\frac{1}{\pi}(2-r),\qquad P^{(3)}(r)=\frac{1}{2\pi}\left(6-6r+r^2\right).$$

For the rest of the paper, we will refer the ODEs of (9) with $\boldsymbol{K}$ replaced by $\boldsymbol{K}^{\delta,(m)}$ the *vortex blob equations* of order m in the plane given by,

$$\boxed{\boldsymbol{F}(\boldsymbol{x},\boldsymbol{y},\dot{\boldsymbol{x}},\dot{\boldsymbol{y}}):=\begin{pmatrix}\left[\dot{x}_i+\frac{h^2}{2\pi}\sum_{j=1,j\neq i}^{M}\omega_j\frac{y_{ij}}{r_{ij}^2}\left(1-Q^{(m)}\left(\frac{r_{ij}^2}{\delta^2}\right)\exp\left(-\frac{r_{ij}^2}{\delta^2}\right)\right)\right]_{1\le i\le M}\\ \left[\dot{y}_i-\frac{h^2}{2\pi}\sum_{j=1,j\neq i}^{M}\omega_j\frac{x_{ij}}{r_{ij}^2}\left(1-Q^{(m)}\left(\frac{r_{ij}^2}{\delta^2}\right)\exp\left(-\frac{r_{ij}^2}{\delta^2}\right)\right)\right]_{1\le i\le M}\end{pmatrix}=\boldsymbol{0},} \tag{13}$$

where $\boldsymbol{x}=(x_1,\ldots,x_M)^T$, $\boldsymbol{y}=(y_1,\ldots,y_M)^T$, and (x_i,y_i) is the position of the i^{th} vortex blob. Furthermore, we used the abbreviations, $x_{ij}=x_i-x_j$, $y_{ij}=y_i-y_j$, and $r_{ij}=\sqrt{x_{ij}^2+y_{ij}^2}$. Beale and Majda showed in [17,18] that the solution to the m^{th} order vortex blob equations converges to the solution of (3a)–(3e) provided that $\delta=h^q$, with $0<q<1$. Moreover, it was shown that the error is of the order $\delta^m=h^{qm}$.

Evidently, the ODEs (13) exhibits a Hamiltonian structure,

$$\omega_i h^2\dot{y}_i=-\frac{\partial\mathcal{H}^{h,(m)}}{\partial x_i},\qquad \omega_i h^2\dot{x}_i=\frac{\partial\mathcal{H}^{h,(m)}}{\partial y_i},$$

where $\mathcal{H}^{h,(m)}(\boldsymbol{x},\boldsymbol{y})$ is the associated Hamiltonian. By Noether's theorem, the translational and rotational symmetry of the Hamiltonian yield the three other conserved quantities, in addition to the Hamiltonian, which are the linear impulse $\boldsymbol{P}$ and angular impulse L. For the $m=2$ case, the conserved quantities are given by,

$$\boldsymbol{\mathcal{P}}^h(\boldsymbol{x},\boldsymbol{y}):=\begin{pmatrix}h^2\sum_{i=1}^{M}\omega_i y_i\\ -h^2\sum_{i=1}^{M}\omega_i x_i\end{pmatrix},\qquad \mathcal{L}^h(\boldsymbol{x},\boldsymbol{y}):=-\frac{h^2}{2}\sum_{i=1}^{M}\omega_i\left(x_i^2+y_i^2\right),$$

$$\mathcal{H}^{h,(2)}(\boldsymbol{x},\boldsymbol{y}):=-\frac{h^4}{4\pi}\sum_{1\le i<j\le M}\omega_i\omega_j\left[\log\left|r_{ij}^2\right|+E_1\left(\frac{r_{ij}^2}{\delta^2}\right)\right].$$

For higher-order vortex blob equations, the expressions for $\boldsymbol{\mathcal{P}}^h$ and $\mathcal{L}^h$ remain the same, only the expression for $\mathcal{H}^{h,(m)}$ changes. Specifically, the Hamiltonians for $m=4,6$ are,

$$\mathcal{H}^{h,(4)}(\boldsymbol{x},\boldsymbol{y}) := -\frac{h^4}{4\pi}\sum_{1\le i<j\le M}\omega_i\omega_j\left[\log\left|r_{ij}^2\right| + E_1\left(\frac{r_{ij}^2}{\delta^2}\right) - \exp\left(-\frac{r_{ij}^2}{\delta^2}\right)\right],$$
$$\mathcal{H}^{h,(6)}(\boldsymbol{x},\boldsymbol{y}) := -\frac{h^4}{4\pi}\sum_{1\le i<j\le M}\omega_i\omega_j\left[\log\left|r_{ij}^2\right| + E_1\left(\frac{r_{ij}^2}{\delta^2}\right) + \left(-\frac{3}{2}+\frac{1}{2}\frac{r_{ij}^2}{\delta^2}\right)\exp\left(-\frac{r_{ij}^2}{\delta^2}\right)\right].$$

Here, $E_1(x)$ denotes the exponential integral and its efficient evaluation up to machine precision will be discussed at the end of Section 3.

2. Discrete Multiplier Method

Before discussing the theory of multiplier method presented in [26], we first fix some notations which will be used throughout the paper.

2.1. Notations and conventions

Let $U \subset \mathbb{R}^d$ and $V \subset \mathbb{R}^{d'}$ be open subsets where here and in the following $d, d', p \in \mathbb{N}$. $f \in C^p(U \to V)$ means f is a p-times continuously differentiable function with domain in U and range in V. We often use boldface to indicate a vectorial quantity $\boldsymbol{f}$. If $\boldsymbol{f} \in C^1(U \to V)$, $\partial_{\boldsymbol{x}}\boldsymbol{f} := \left[\frac{\partial f_i}{\partial x_j}\right]$ denotes the Jacobian matrix. Let $I \subset \mathbb{R}$ be an open interval and let $\boldsymbol{x} \in C^1(I \to U)$, $\dot{\boldsymbol{x}}$ denote the derivative with respect to time $t \in I$. Also if $\boldsymbol{x} \in C^p(I \to U)$, $\boldsymbol{x}^{(q)}$ denotes the q-th time derivative of $\boldsymbol{x}$ for $1 \le q \le p$. For brevity, the explicit dependence of $\boldsymbol{x}$ on t is often omitted with the understanding that $\boldsymbol{x}$ is to be evaluated at t. If $\boldsymbol{\psi} \in C^1(I \times U \to V)$, $D_t\boldsymbol{\psi}$ denotes the total derivative[1] with respect to t, and $\partial_t\boldsymbol{\psi}$ denotes the partial derivative with respect to t. $M_{d'\times d}(\mathbb{R})$ denotes the set of all $d' \times d$ matrices with real entries.

2.2. Conserved quantities of quasilinear first order ODEs

Consider a quasilinear first-order system of ODEs,

$$\boldsymbol{F}(t,\boldsymbol{x},\dot{\boldsymbol{x}}) := \dot{\boldsymbol{x}}(t) - \boldsymbol{f}(t,\boldsymbol{x}) = \boldsymbol{0}, \qquad \boldsymbol{x}(t_0) = \boldsymbol{x}_0, \tag{14}$$

where $t \in I$, $\boldsymbol{x} = (x_1(t), \dots, x_n(t)) \in U$. For $1 \le p \in \mathbb{N}$, if $\boldsymbol{f} \in C^{p-1}(I \times U \to \mathbb{R}^n)$ and is Lipschitz continuous in U, then standard ODE theory implies there exists an unique solution $\boldsymbol{x} \in C^p(I \to U)$ to the first-order system (14) in a neighborhood of $(t_0, \boldsymbol{x}_0) \in I \times U$.

Definition 1. Let $d' \in \mathbb{N}$ with $1 \le d' \le d$. A vector-valued function $\boldsymbol{\psi} \in C^1(I \times U \to \mathbb{R}^{d'})$ is a vector of conserved quantities[2] (or equivalently first integrals) if

$$D_t\boldsymbol{\psi}(t,\boldsymbol{x}) = \boldsymbol{0}, \text{ for any } t \in I \text{ and } C^1(I \to U) \text{ solution } \boldsymbol{x} \text{ of } (14). \tag{15}$$

In other words, $\boldsymbol{\psi}(t,\boldsymbol{x})$ is constant on any $C^1(I \to U)$ solution $\boldsymbol{x}$ of (14).

A generalization of integrating factors is known as *characteristics* by [32] or equivalently, *conservation law multipliers* by [28]. We will adopt the terminology of conversation law multiplier or just multiplier when the context is clear.

Definition 2. Let $d' \in \mathbb{N}$ with $1 \le d' \le d$ and $U^{(1)}$ be an open subset of $\mathbb{R}^d$. A conservation law multiplier of $\boldsymbol{F}$ is a matrix-valued function $\Lambda \in C(I \times U \times U^{(1)} \to M_{d'\times d}(\mathbb{R}))$ such that there exists a function $\boldsymbol{\psi} \in C^1(I \times U \to \mathbb{R})$ satisfying,

$$\Lambda(t,\boldsymbol{x},\dot{\boldsymbol{x}})(\dot{\boldsymbol{x}}(t) - \boldsymbol{f}(t,\boldsymbol{x})) = D_t\boldsymbol{\psi}(t,\boldsymbol{x}), \text{ for } t \in I, \boldsymbol{x} \in C^1(I \to U). \tag{16}$$

Here, we emphasize that condition (16) is satisfied as an identity for arbitrary C^1 functions $\boldsymbol{x}$; in particular $\boldsymbol{x}$ need not be a solution of (14). It follows from the definition of conservation law multiplier that existence of multipliers implies existence of conservation laws. Conversely, given a known vector of conserved quantities $\boldsymbol{\psi}$, there can be many conservation law multipliers which correspond to $\boldsymbol{\psi}$. It was shown in [26] that it suffices to consider multipliers of the form $\Lambda(t,\boldsymbol{x})$ where a one-to-one correspondence exists between conservation law multipliers and conserved quantities of (14).

[1] In the context of fluid dynamics, this can also be called the material derivative.
[2] By quasilinearity of (14), it suffices to consider conserved quantities depending only on $t, \boldsymbol{x}$, see [26].

Theorem 1 *(Theorem 4 of [26]). Let* $\boldsymbol{\psi} \in C^1(I \times U \to \mathbb{R}^{d'})$*. Then there exists a unique conservation law multiplier of* (14) *of the form* $\Lambda \in C(I \times U \to M_{d' \times d}(\mathbb{R}))$ *associated with the function* $\boldsymbol{\psi}$ *if and only if* $\boldsymbol{\psi}$ *is a conserved quantity of* (14)*. And if so,* Λ *is unique and satisfies for any* $t \in I$ *and* $\boldsymbol{x} \in C^1(I \to U)$*,*

$$\Lambda(t, \boldsymbol{x}) = \partial_{\boldsymbol{x}} \boldsymbol{\psi}(t, \boldsymbol{x}), \tag{17a}$$

$$\Lambda(t, \boldsymbol{x}) \boldsymbol{f}(t, \boldsymbol{x}) = -\partial_t \boldsymbol{\psi}(t, \boldsymbol{x}). \tag{17b}$$

To construct conservative methods for (14) with conserved quantities (15), we shall discretize the time interval I by a uniform time size $\tau \in \mathbb{R}$, i.e. $t^{k+1} = t^k + \tau$ for $k \in \mathbb{N}$, and focus on one-step conservative methods.[3] First, we recall some definitions from [26].

Definition 3. Let W be a normed vector space, such as $\mathbb{R}^{d'}$ with the Euclidean norm or $M_{d' \times d}(\mathbb{R})$ with the operator norm. A function $g^\tau : I \times U \times U \to W$ is called a one-step function if g^τ depends only on $t^k \in I$ and the discrete approximations $\boldsymbol{x}^{k+1}, \boldsymbol{x}^k \in U$.

Definition 4. A sufficiently smooth one-step function $g^\tau : I \times U \times U \to W$ is consistent to a sufficiently smooth $g : I \times U \times U^{(1)} \to W$ if for any $\boldsymbol{x} \in C^2(I \to U)$, there is a constant $C > 0$ independent of τ so that $\left\| g(t^k, \boldsymbol{x}(t^k), \dot{\boldsymbol{x}}(t^k)) - g^\tau(t^k, \boldsymbol{x}(t^{k+1}), \boldsymbol{x}(t^k)) \right\|_W \leq C \left\| \boldsymbol{x} \right\|_{C^2([t^k, t^{k+1}])} \tau$, where $\left\| \boldsymbol{x} \right\|_{C^2([t^k, t^{k+1}])} := \max_{0 \le i \le 2} \left\| \boldsymbol{x}^{(i)} \right\|_{L^\infty([t^k, t^{k+1}])}$. If so, we write $g^\tau = g + \mathcal{O}(\tau)$.

We shall be considering the following consistent one–step functions for $\dot{\boldsymbol{x}}, D_t \boldsymbol{\psi}, \partial_t \boldsymbol{\psi}$:

$$D_t^\tau \boldsymbol{x}(t^k, \boldsymbol{x}^{k+1}, \boldsymbol{x}^k) := \frac{\boldsymbol{x}^{k+1} - \boldsymbol{x}^k}{\tau} = \dot{x} + \mathcal{O}(\tau), \tag{18}$$

$$D_t^\tau \boldsymbol{\psi}(t^k, \boldsymbol{x}^{k+1}, \boldsymbol{x}^k) := \frac{\boldsymbol{\psi}(t^{k+1}, \boldsymbol{x}^{k+1}) - \boldsymbol{\psi}(t^k, \boldsymbol{x}^k)}{\tau} = D_t \boldsymbol{\psi} + \mathcal{O}(\tau), \tag{19}$$

$$\partial_t^\tau \boldsymbol{\psi}(t^k, \boldsymbol{x}^{k+1}, \boldsymbol{x}^k) := \frac{\boldsymbol{\psi}(t^{k+1}, \boldsymbol{x}^k) - \boldsymbol{\psi}(t^k, \boldsymbol{x}^k)}{\tau} = \partial_t \boldsymbol{\psi} + \mathcal{O}(\tau). \tag{20}$$

Definition 5. Let $\boldsymbol{f}^\tau$ be a consistent 1-step function to $\boldsymbol{f}$. We say that the 1-step method,

$$D_t^\tau \boldsymbol{x}(t^k, \boldsymbol{x}^{k+1}, \boldsymbol{x}^k) = \boldsymbol{f}^\tau(t^k, \boldsymbol{x}^{k+1}, \boldsymbol{x}^k) \tag{21}$$

is conservative in $\boldsymbol{\psi}$, if $\boldsymbol{\psi}(t^{k+1}, \boldsymbol{x}^{k+1}) = \boldsymbol{\psi}(t^k, \boldsymbol{x}^k)$ on any solution $\boldsymbol{x}^{k+1}$ of (21) and $k \in \mathbb{N}$.

We now state two key conditions from [26] for constructing conservative 1-step methods, which can be seen as a discrete analog of (17a) and (17b).

Theorem 2 *(Theorem 17 of [26]). Let* $D_t^\tau \boldsymbol{x}, D_t^\tau \boldsymbol{\psi}, \partial_t^\tau \boldsymbol{\psi}$ *be as defined in* (18)–(20)*. And let* Λ *be the conservation law multiplier of* (14) *associated with a conserved quantity* $\boldsymbol{\psi}$*. If* $\boldsymbol{f}^\tau$ *and* Λ^τ *are consistent* 1*-step functions to* $\boldsymbol{f}, \Lambda$ *satisfying*

$$\Lambda^\tau D_t^\tau \boldsymbol{x} = D_t^\tau \boldsymbol{\psi} - \partial_t^\tau \boldsymbol{\psi}, \tag{22a}$$

$$\Lambda^\tau \boldsymbol{f}^\tau = -\partial_t^\tau \boldsymbol{\psi}, \tag{22b}$$

then the 1*-step method defined by* (21) *is conservative in* $\boldsymbol{\psi}$*.*

In [26], condition (22a) was solved by the use of divided difference calculus and (22b) was solved using a local matrix inversion formula. For the vortex blob equations (13), we follow the approach employed by [1] and directly verify (22a) and (22b) for specific choices of $\boldsymbol{f}^\tau$ and Λ^τ. Before we end this section, we mention a well-known result for even order of accuracy for symmetric schemes. For more details, one can see Chapter II.3 of [5].

Definition 6 *(Symmetric schemes [5]).* Let Φ^τ be the discrete flow of a one-step numerical method for system (14) with time step τ. The associated adjoint method $\left(\Phi^\tau\right)^*$ of the one-step method Φ^τ is the inverse of the original method with reversed time step $-\tau$, i.e. $\left(\Phi^\tau\right)^* = \left(\Phi^{-\tau}\right)^{-1}$. A method is symmetric if $\left(\Phi^\tau\right)^* = \Phi^\tau$.

Theorem 3 *(Theorem II-3.2 of [5]). A symmetric method is of even order.*

[3] Analogous results hold for variable time step sizes and multi-step methods, see [26,12] for more details.

3. Construction of exactly conservative integrators via DMM

In [1], conservative schemes for the *point vortex equations* in the plane were derived using DMM preserving the four analogous conserved quantities. Here, we will extend their results and derive conservative schemes for the *vortex blob equations* of order 2, 4, and 6 from Equation (13).

Before deriving the schemes, we first verify that $\mathcal{P}^h$, $\mathcal{L}^h$, $\mathcal{H}^{h,(m)}$ are indeed the conserved quantities of (13) using Theorem 1. Let us define the vector of conserved quantities $\boldsymbol{\psi}^h$ as,

$$\boldsymbol{\psi}^h(\boldsymbol{x},\boldsymbol{y}) := \begin{pmatrix} \mathcal{P}^h(\boldsymbol{x},\boldsymbol{y}) \\ \mathcal{L}^h(\boldsymbol{x},\boldsymbol{y}) \\ \mathcal{H}^{h,(m)}(\boldsymbol{x},\boldsymbol{y}) \end{pmatrix}.$$

Using condition (17a), this yields the $4\times(2M)$ multiplier matrix Λ given by,

$$\Lambda(\boldsymbol{x},\boldsymbol{y}) := \begin{pmatrix} [0]^T_{1\le i\le M} & \left[h^2\omega_i\right]^T_{1\le i\le M} \\ \left[-h^2\omega_i\right]^T_{1\le i\le M} & [0]^T_{1\le i\le M} \\ \left[-h^2\omega_i x_i\right]^T_{1\le i\le M} & \left[-h^2\omega_i y_i\right]^T_{1\le i\le M} \\ \left[-\frac{h^4}{2\pi}\omega_i\sum_{j=1,j\neq i}^{M}\omega_j x_{ij}\frac{C^{(m)}_{ij}}{r^2_{ij}}\right]^T_{1\le i\le M} & \left[-\frac{h^4}{2\pi}\omega_i\sum_{j=1,j\neq i}^{M}\omega_j y_{ij}\frac{C^{(m)}_{ij}}{r^2_{ij}}\right]^T_{1\le i\le M} \end{pmatrix},$$

where $C^{(m)}_{ij} := C^{(m)}\left(r^2_{ij}\right) = 1 - Q^{(m)}\left(\frac{r^2_{ij}}{\delta^2}\right)\exp\left(-\frac{r^2_{ij}}{\delta^2}\right)$.

We showed the details on how condition (17b) is satisfied in Appendix A.1, which verifies that $\boldsymbol{\psi}^h$ is indeed conserved quantities by Theorem 1. Next, we propose consistent choices of $D^\tau_t\boldsymbol{x}$, $D^\tau_t\boldsymbol{\psi}^h$, $\partial^\tau_t\boldsymbol{\psi}^h$, Λ^τ, and $\boldsymbol{f}^\tau$, then verify that conditions (22a) and (22b) are satisfied. Specifically, we define,

$$D^\tau_t\boldsymbol{x} := \frac{1}{\tau}\begin{pmatrix}\Delta\boldsymbol{x}\\ \Delta\boldsymbol{y}\end{pmatrix},\quad D^\tau_t\boldsymbol{\psi}^h := \frac{1}{\tau}\begin{pmatrix}\Delta\mathcal{P}^h(\boldsymbol{x},\boldsymbol{y})\\ \Delta\mathcal{L}^h(\boldsymbol{x},\boldsymbol{y})\\ \Delta\mathcal{H}^{h,(m)}(\boldsymbol{x},\boldsymbol{y})\end{pmatrix},\quad \partial^\tau_t\boldsymbol{\psi}^h := \boldsymbol{0}.$$

As well, we define the discrete multiplier matrix Λ^τ and the discrete right hand side $\boldsymbol{f}^\tau$ as,

$$\Lambda^\tau\left(\boldsymbol{x}^{k+1},\boldsymbol{y}^{k+1},\boldsymbol{x}^k,\boldsymbol{y}^k\right) :=$$

$$\begin{pmatrix} [0]^T_{1\le i\le M} & \left[h^2\omega_i\right]^T_{1\le i\le M} \\ \left[-h^2\omega_i\right]^T_{1\le i\le M} & [0]^T_{1\le i\le M} \\ \left[-h^2\omega_i\overline{x_i}\right]^T_{1\le i\le M} & \left[-h^2\omega_i\overline{y_i}\right]^T_{1\le i\le M} \\ \left[-\frac{h^4}{2\pi}\omega_i\sum_{j=1,j\neq i}^{M}\omega_j\frac{\overline{x_{ij}}}{\left(r^k_{ij}\right)^2}C^{\tau,(m)}_{ij}\right]^T_{1\le i\le M} & \left[-\frac{h^4}{2\pi}\omega_i\sum_{j=1,j\neq i}^{M}\omega_j\frac{\overline{y_{ij}}}{\left(r^k_{ij}\right)^2}C^{\tau,(m)}_{ij}\right]^T_{1\le i\le M} \end{pmatrix},$$

$$\boldsymbol{f}^\tau\left(\boldsymbol{x}^{k+1},\boldsymbol{y}^{k+1},\boldsymbol{x}^k,\boldsymbol{y}^k\right) := \begin{pmatrix} \left[-\frac{h^2}{2\pi}\sum_{j=1,j\neq i}^{M}\omega_j\frac{\overline{y_{ij}}}{\left(r^k_{ij}\right)^2}C^{\tau,(m)}_{ij}\right]_{1\le i\le M} \\ \left[\frac{h^2}{2\pi}\sum_{j=1,j\neq i}^{M}\omega_j\frac{\overline{x_{ij}}}{\left(r^k_{ij}\right)^2}C^{\tau,(m)}_{ij}\right]_{1\le i\le M} \end{pmatrix},$$

where $\overline{x_i} := (x^{k+1}_i + x^k_i)/2$, $\overline{y_i} := (y^{k+1}_i + y^k_i)/2$, $\overline{x_{ij}} := (x^{k+1}_{ij} + x^k_{ij})/2$, $\overline{y_{ij}} := (y^{k+1}_{ij} + y^k_{ij})/2$,

$$C^{\tau,(2)}_{ij} = \frac{1}{\frac{\xi^{k+1}_{ij}}{\xi^k_{ij}} - 1}\left[\log\left|\frac{\xi^{k+1}_{ij}}{\xi^k_{ij}}\right| + E_1\left(\xi^{k+1}_{ij}\right) - E_1\left(\xi^k_{ij}\right)\right],$$

$$C_{ij}^{\tau,(4)} = \frac{1}{\frac{\xi_{ij}^{k+1}}{\xi_{ij}^{k}} - 1}\left[\log\left|\frac{\xi_{ij}^{k+1}}{\xi_{ij}^{k}}\right| + E_1\left(\xi_{ij}^{k+1}\right) - E_1\left(\xi_{ij}^{k}\right) - e^{-\xi_{ij}^{k}}\left(e^{-\Delta\xi_{ij}} - 1\right)\right],$$

$$C_{ij}^{\tau,(6)} = \frac{1}{\frac{\xi_{ij}^{k+1}}{\xi_{ij}^{k}} - 1}\left[\log\left|\frac{\xi_{ij}^{k+1}}{\xi_{ij}^{k}}\right| + E_1\left(\xi_{ij}^{k+1}\right) - E_1\left(\xi_{ij}^{k}\right) + e^{-\xi_{ij}^{k}}\left(e^{-\Delta\xi_{ij}} - 1\right)\left(-\frac{3}{2} + \frac{1}{2}\xi_{ij}^{k}\right)\right] + \frac{1}{2}\xi_{ij}^{k}e^{-\xi_{ij}^{k+1}},$$

and $\xi_{ij}^{k} := (r_{ij}^{k}/\delta)^2$. As before, we verify that conditions (22a) and (22b) hold in Appendix A.2 and A.3. Thus, we have derived the conservative discretization for (13) which exactly preserves $\boldsymbol{\psi}$ given by,

$$\boldsymbol{F}^{\tau}\left(\boldsymbol{x}^{k+1}, \boldsymbol{y}^{k+1}, \boldsymbol{x}^{k}, \boldsymbol{y}^{k}\right) := \begin{pmatrix} \left[\dfrac{x_i^{k+1} - x_i^{k}}{\tau} + \dfrac{h^2}{2\pi}\displaystyle\sum_{j=1, j\neq i}^{M}\omega_j \dfrac{\overline{y_{ij}}}{\left(r_{ij}^{k}\right)^2} C_{ij}^{\tau,(m)}\right]_{1\leq i\leq M} \\ \left[\dfrac{y_i^{k+1} - y_i^{k}}{\tau} - \dfrac{h^2}{2\pi}\displaystyle\sum_{j=1, j\neq i}^{M}\omega_j \dfrac{\overline{x_{ij}}}{\left(r_{ij}^{k}\right)^2} C_{ij}^{\tau,(m)}\right]_{1\leq i\leq M} \end{pmatrix} = \boldsymbol{0}. \tag{23}$$

Moreover, we show that the above scheme is symmetric in Appendix A.4, which is consistent with 2nd order accuracy shown later in Section 4. It is important to mention that, when any two vortices i and j move in such a way that $r_{ij}^{k} = r_{ij}^{k+1}$, the numerator and denominator of $C_{ij}^{\tau,(m)}$ may tend to zero, potentially leading to large round-off errors. Thus, in our implementation, we replace the expressions for $C_{ij}^{\tau,(m)}$ by their truncated Taylor expansions when $|(r_{ij}^{k+1}/r_{ij}^{k})^2 - 1| \leq \varepsilon$, where $\varepsilon = 10^{-4}$. Specifically, the Taylor expansions of $C_{ij}^{\tau,(m)}$ with $m = 2, 4, 6$ are respectively given by,

$$\begin{aligned} C_{ij}^{\tau,(2)} = {} & \left(1 - e^{-\xi_{ij}^{k}}\right) + \frac{(z_{ij}-1)}{2}\left(-1 + \left(1 + \xi_{ij}^{k}\right)e^{-\xi_{ij}^{k}}\right) + \\ & \frac{(z_{ij}-1)^2}{6}\left(2 + \left(-2 - 2\xi_{ij}^{k} - \left(\xi_{ij}^{k}\right)^2\right)e^{-\xi_{ij}^{k}}\right) + \ldots, \\ C_{ij}^{\tau,(4)} = {} & \left(1 + \left(-1 + \xi_{ij}^{k}\right)e^{-\xi_{ij}^{k}}\right) + \frac{(z_{ij}-1)}{2}\left(-1 + \left(1 + \xi_{ij}^{k} - \left(\xi_{ij}^{k}\right)^2\right)e^{-\xi_{ij}^{k}}\right) + \\ & \frac{(z_{ij}-1)^2}{6}\left(2 + \left(-2 - 2\xi_{ij}^{k} - \left(\xi_{ij}^{k}\right)^2 + \left(\xi_{ij}^{k}\right)^3\right)e^{-\xi_{ij}^{k}}\right) + \ldots, \\ C_{ij}^{\tau,(6)} = {} & \left(1 + \left(-1 + 2\xi_{ij}^{k} + \frac{1}{2}\left(\xi_{ij}^{k}\right)^2\right)e^{-\xi_{ij}^{k}}\right) + \\ & \frac{(z_{ij}-1)}{2}\left(-2 + \left(2 + 2\xi_{ij}^{k} - 5\left(\xi_{ij}^{k}\right)^2 + \left(\xi_{ij}^{k}\right)^3\right)e^{-\xi_{ij}^{k}}\right) + \\ & \frac{(z_{ij}-1)^2}{6}\left(4 + \left(-4 - 4\xi_{ij}^{k} - 2\left(\xi_{ij}^{k}\right)^2 + 6\left(\xi_{ij}^{k}\right)^3 - \left(\xi_{ij}^{k}\right)^4\right)e^{-\xi_{ij}^{k}}\right) + \ldots, \end{aligned}$$

where $z_{ij} = (r_{ij}^{k+1}/r_{ij}^{k})^2 = \xi_{ij}^{k+1}/\xi_{ij}^{k}$. From these expansions, it can be seen that both Λ^{τ} and $\boldsymbol{f}^{\tau}$ are consistent because, as $\tau \to 0$ we have $\overline{x_{ij}} \to x_{ij}$ and $\overline{y_{ij}} \to y_{ij}$, along with $z_{ij} \to 1$ which results in $C_{ij}^{\tau,(2)} \to C_{ij}^{(2)}$, $C_{ij}^{\tau,(4)} \to C_{ij}^{(4)}$, and $C_{ij}^{\tau,(6)} \to C_{ij}^{(6)}$. As discussed above on our implementations, we truncate the Taylor series expansions of $C_{ij}^{\tau,(2)}$, $C_{ij}^{\tau,(4)}$, and $C_{ij}^{\tau,(6)}$ at 3rd term (2nd order). In Appendix A.5, we further verify the accuracy of our Taylor expansions, and demonstrate how round-off errors appear as $(r_{ij}^{k+1}/r_{ij}^{k})^2 \to 1$ justifying our choice of ε.

Finally, in order to implement the conservative schemes given by (23), one must be able to evaluate the exponential integral

$$E_1(x) = \int_{x}^{\infty} \frac{e^{-t}}{t}\,dt, \quad x > 0,$$

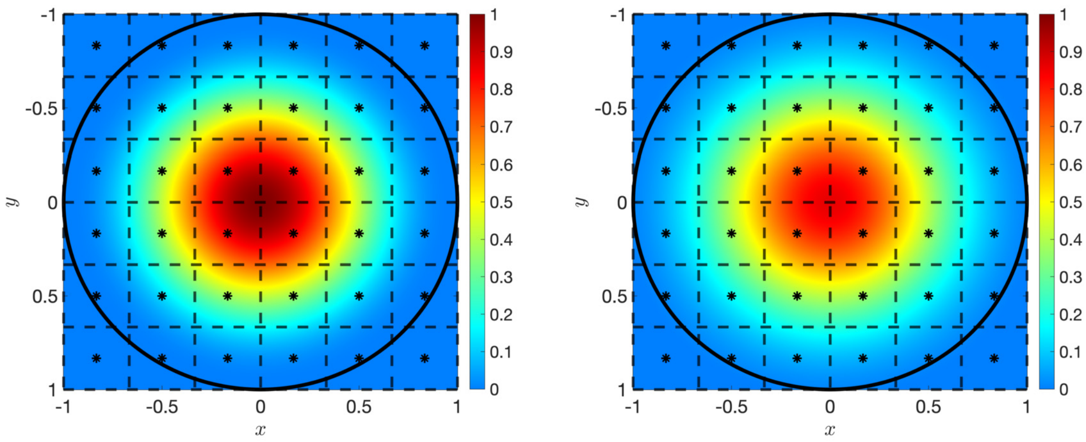

Fig. 4.1. The discretization of Ω and ω_0 with $M = 36$ vortices. Black stars show the location of vortices, dashed lines form the grid, the black circle is the boundary $\partial\Omega$, and the color of a point together with the colorbar represents the intensity of the vorticity field at that point. On the left, we have the exact vorticity field before introducing the vortices. While on the right, we have the approximate vorticity field given by (12) for $m = 4$ after introducing the vortices. (For interpretation of the colors in the figure(s), the reader is referred to the web version of this article.)

up to machine precision in an efficient manner. Various methods of evaluating the exponential integral exist, such as Taylor series expansion, asymptotic expansion, continued fraction expansion, and piece-wise rational function approximation [33, 34]. We want to be able to evaluate $E_1(x)$ for a wide range of input arguments. This is due to the possibility that the argument x can be very small when vortices converge to a particular point in space, and can be very large when vortices diverge to infinity from a particular point in space, or when we let $\delta \to 0$. It is known that for $x > 34$, we have $|E_1(x)| < 10^{-16}$ which suggests that we want to look for a fast and accurate algorithm for evaluating $E_1(x)$ in the range $10^{-16} < x < 34$. As the rate of convergence and the accuracy of evaluating the exponential integral vary with the input argument, after numerical testing, we have chosen to use the rational function approximation [34] to evaluate $E_1(x)$ when implementing the conservative discretizations. The rational function approach provides a inexpensive and accurate means of evaluating $E_1(x)$ over the desired range of input arguments.

4. Numerical results

Before presenting numerical results in detail, we first mention that we conducted all our experiments in C using a 1.6 GHz Intel Core i5 dual-core processor. We did not optimize our codes for parallel computing, as we wished to focus on verifying specific properties about the conservative schemes.

Since the scheme in (23) is nonlinear and implicit, we used fixed-point iterations to solve for $\boldsymbol{x}^{k+1}$ and $\boldsymbol{y}^{k+1}$ given $\boldsymbol{x}^k$ and $\boldsymbol{y}^k$ in our implementations. We let the initial guess for our fixed point iterations to be the result of taking an RK4 step from $(\boldsymbol{x}^k, \boldsymbol{y}^k)$.

All our numerical experiments will be based on solving (3a)–(3e) with initial vorticity field given by,

$$\omega_0(r) = \begin{cases} \left(1-r^2\right)^3 & r \le 1 \\ 0 & r > 1. \end{cases} \tag{24}$$

We define our domain Ω to be the square described by $(x, y) \in [-1, 1] \times [-1, 1]$. We discretize Ω with a uniform grid with size $h = 2/\sqrt{M}$, where M is the number of vortices. Then, we introduce a vortex at the center of each square such that i^{th} vortex has vorticity $\omega_i = \omega_0(r_i)$. Fig. 4.1 depicts the discretization of Ω with 36 vortices. On the left, we have 36 vortices placed on Ω as described, where the vorticity field on Ω is given by $\omega_0(r)$ at any point. On the right, we have the same vortices placed on Ω, yet the vorticity field on Ω is given by $\omega_0^h(r)$.

We discretize the vortex blob equations resulting from applying the vortex blob method to (3a)–(3e) using (23). In doing so, we set $m = 4$ and $\delta = h^q$ with $q = 0.75$. We let $\{t^k\}_{k=0}^M$ be the temporal grid points and $T = t^N$ be the final time, where N is the total number of time steps our integrator will take. Later in this section, we will verify the temporal order of convergence of the conservative integrators and the spatial order of convergence of the vortex blob method. To perform such verification efficiently, we will need the analytical solution to (3a)–(3e) with the $\omega_0^h(r)$ given in (24). We can obtain the analytical solution by exploiting the rotational symmetry of the initial vorticity field. Since the Laplacian ∇^2 is rotationally invariant, the velocity field satisfying (3a)–(3e) is also be rotationally symmetric and is given by,

$$\boldsymbol{v}(\boldsymbol{z}) = \frac{1}{r^2}[-y,\ x]^T \int_0^r s\omega(s)\,ds = [-y,\ x]^T\ \frac{1-\left(1-r^2\right)^4}{8r^2}. \tag{25}$$

Thus, we expect vortex trajectories to form concentric circles.

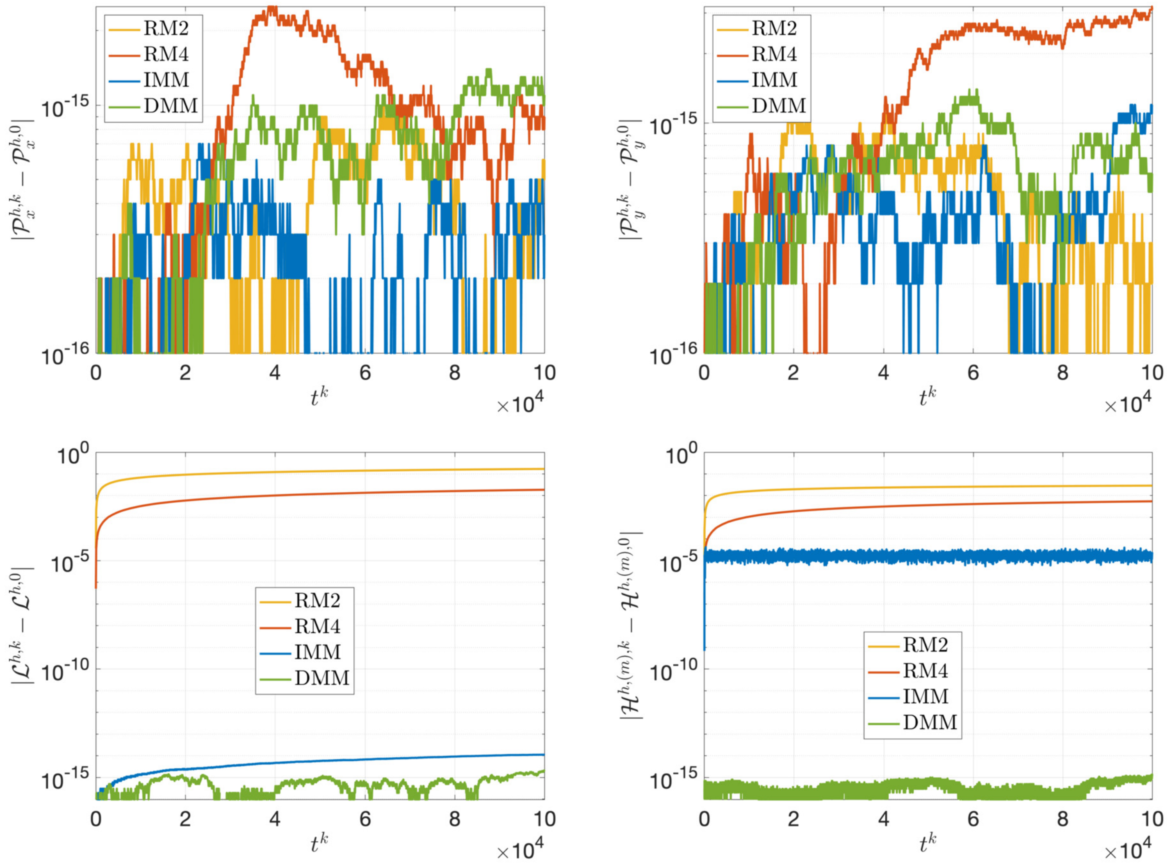

Fig. 4.2. Error over time in conserved quantities $\mathcal{P}_x^h$ (top-left), $\mathcal{P}_y^h$ (top-right), $\mathcal{L}^h$ (bottom-left), and $\mathcal{H}^{h,(m)}$ (bottom-right) for m^{th} order vortex method. Here, (13) was solved with $m = 4$, $M = 100$, $T = 10^5$, and $\tau = 1.0$ using RM2, RM4, IMM, and DMM.

4.1. Verification and comparison of conservative properties

We start by comparing the error over time in conserved quantities of $\boldsymbol{\mathcal{P}}^h$, $\mathcal{L}^h$, and $\mathcal{H}^{h,(m)}$ for the DMM-based discretization in (23) with discretizations of (13) obtained via Ralston's 2nd and 4th order method (RM2, RM4), and the implicit midpoint method (IMM). In our comparisons, we use Ralston's methods due to their minimal truncation error bounds of Lotkin type [35,36]. Fig. 4.2 shows how the drift (i.e., $|\psi^{h,k} - \psi^{h,0}|$) in all four conserved quantities evolves with time. It can be observed that all integrators preserve linear impulses at the discrete level. On the other hand, we see that only DMM and implicit midpoint method conserve angular momentum. This is not surprising as DMM is conservative by construction and the implicit midpoint method preserved all quadratic invariants [5]. As expected, the only integrator that conserves Hamiltonian up to machine precision, and as a result all four conserved quantities, is DMM. Although IMM does not exactly preserve the Hamiltonian, we see that its Hamiltonian error remains bounded below 10^{-4}. This is expected, as it is well known that for an r^{th} order symplectic method, the error in Hamiltonian is $O(\tau^r)$ over an exponentially long time [5].

4.1.1. Convergence analysis of conserved quantities to conserved integrals

In this subsection, we will show that conservative property of the derived schemes has two important theoretical implications. First is that the error between the conserved quantities of the vortex blob equations (13) and the conserved integrals of Euler's equations (3a)–(3e) remains bounded for an arbitrarily long time. Secondly, the conserved quantities of (13) converge to the conserved integrals of (3a)–(3e) as $M \to \infty$.

Let ψ be the exact value of the conserved integral $\psi[\omega](t)$ of (3a)–(3e) (e.g., $\mathcal{P}_x$, $\mathcal{P}_y$, $\mathcal{L}$, or $\mathcal{H}^{(m)}$) with the corresponding discretized conserved quantity ψ^h of (13). For fixed τ and T, we expect the conserved quantity $\psi^{h,N}$ to converge to ψ as $h \to 0$. We will demonstrate that this is indeed the case when we employ the DMM-based discretizations (23). Specifically, recall that $\psi^h(\boldsymbol{x}(t), \boldsymbol{y}(t))$ is the conserved quantity evaluated on the exact solution of (13) that satisfies the initial conditions $\boldsymbol{x}(0) = \boldsymbol{x}^0$ and $\boldsymbol{y}(0) = \boldsymbol{y}^0$. Then, $\psi^h(\boldsymbol{x}(t^N), \boldsymbol{y}(t^N)) = \psi^h\left(\boldsymbol{x}^0, \boldsymbol{y}^0\right) = \psi^{h,0}$, and from triangle inequality we have,

$$\left|\psi^{h,N} - \psi\right| \le \left|\psi^{h,0} - \psi\right| + \left|\psi^{h,N} - \psi^{h,0}\right|$$

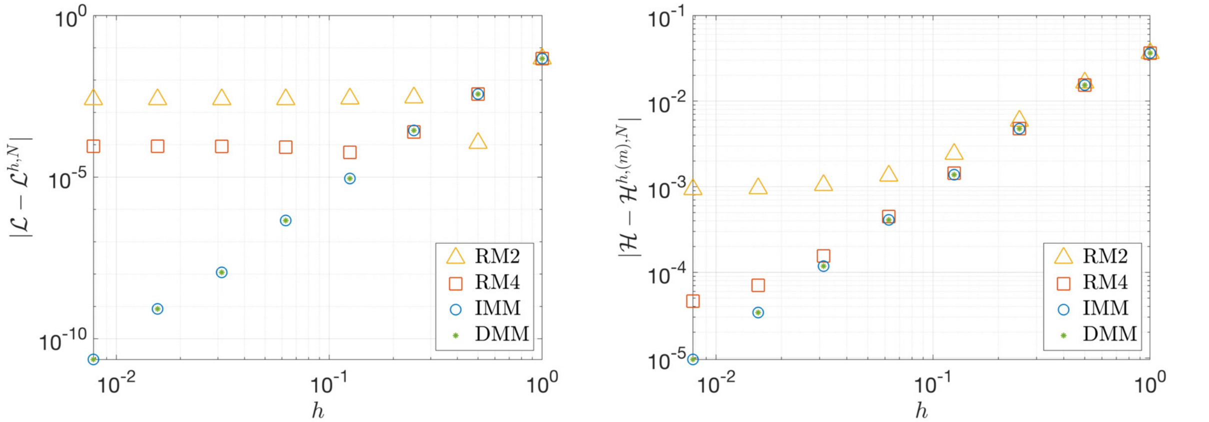

Fig. 4.3. Convergence of $\mathcal{L}^{h,N}$ to $\mathcal{L}$ (left), and the convergence of $\mathcal{H}^{h,(m),N}$ to $\mathcal{H}$ (right) as $h \to 0$ when (13) is solved with $m = 4$, $T = 10$, and $\tau = 1.0$ using RM2, RM4, IMM, and DMM.

$$\leq \left|\psi^{h,0} - \psi\right| + \left|\psi^{h,N} - \psi^h\left(\boldsymbol{x}(t^N), \boldsymbol{y}(t^N)\right)\right|$$
$$\leq \underbrace{\left|\psi^{h,0} - \psi\right|}_{\boxed{1}} + L_{\psi^h} \underbrace{\left\| \begin{bmatrix} \boldsymbol{x}^N \\ \boldsymbol{y}^N \end{bmatrix} - \begin{bmatrix} \boldsymbol{x}(t^N) \\ \boldsymbol{y}(t^N) \end{bmatrix} \right\|}_{\boxed{2}},$$

where the third line follows from assuming that $\psi^h(\boldsymbol{x}, \boldsymbol{y})$ is Lipschitz continuous with Lipschitz constant L_ψ. Observe that,

- $\boxed{1}$ is simply the error between ψ and the midpoint rule approximation of $\psi[\omega](t)$ if $\psi^h = \mathcal{P}_x^h$, $\mathcal{P}_y^h$, or $\mathcal{L}^h$. Therefore, when ψ represents $\mathcal{P}_x$, $\mathcal{P}_y$, or $\mathcal{L}$, $|\psi^{h,0} - \psi|$ is $O\left(h^2\right)$. $\mathcal{H}^{h,(m),0}$ is also the midpoint sum approximating $\mathcal{H}$ when $m = 0$ (point vortex case), but this is not true for all m. This is because, unlike $\mathcal{H}[\omega](t)$, $\mathcal{H}^{h,(m)}$ contains an exponential integral term and exponential terms. Nonetheless, it is easy to show[4] that these extra terms decay exponentially as $h \to 0$, implying that $|\psi^{h,0} - \psi|$ is still $O\left(h^2\right)$ when ψ^h is $\mathcal{H}^{h,(m)}$ with $m = 2, 4, 6$.
- $\boxed{2}$ is the error between the numerical solution and the exact solution of (13) at $t = t^N = T$. For an r^{th} order integrator it is $O\left(\tau^r\right)$.

Therefore, we have,

$$\left|\psi^{h,N} - \psi\right| \leq C_1 h^2 + C_2 L_\psi \tau^r \tag{26}$$

for ψ is $\mathcal{P}_x$, $\mathcal{P}_y$, $\mathcal{L}$, or $\mathcal{H}$ with C_1 and C_2 as some positive constants. When the conservative integrators are employed, $|\psi^{h,N} - \psi^{h,0}|$ is analytically nil, and practically of the same order as machine epsilon (ε_M). Therefore, for conservative integrators of (23), we have a tighter bound than (26) which is independent of τ and given by,

$$\left|\psi^{h,N} - \psi\right| \leq C_1 h^2 + g\left(\varepsilon_M, N\right).$$

Here, $g\left(\varepsilon_M, N\right)$ can be viewed as a unknown random variable that models the accumulation of round-off/truncation errors due to finite-precision arithmetic when using (23). Thus, $\psi^{h,N}$ should converge to ψ with second order accuracy as $h \to 0$ for all $N > 0$ when we integrate (13) using (23). On the other hand, if we use a non-conservative integrator like RM2, RM4, or IMM, $\psi^{h,N}$ should stop converging to ψ as $h \to 0$ for all $N > 0$ because τ^r term will dominate over h^2 term for sufficiently small h. We demonstrate this behavior numerically in Fig. 4.3.

From Fig. 4.3, it can be seen that the errors $|\mathcal{L}^{h,N} - \mathcal{L}|$ of RM2 and RM4 plateau, as h tends to zero. As expected, since IMM and DMM preserve angular momentum, their errors $|\mathcal{L}^{h,N} - \mathcal{L}|$ decrease monotonically. Although (26) implies that we should also see plateaus in the errors of $|\mathcal{H}^{h,(m),N} - \mathcal{H}|$ for RM2, RM4, and IMM, we observe plateaus only in the curves of RM2 and RM4 of Fig. 4.3. If h were to be decreased further, we expect to see the plateau for IMM also. However, we did not pursue this further due to costly simulation, due the spatial dominance in the error.

[4] Conserved quantities $\boldsymbol{\mathcal{P}}^h$ and $\mathcal{L}^h$ are the discrete and per unit mass versions of the conserved integrals (6) and (7). Likewise, $\mathcal{H}^{h,(m)}$ are the discrete and per unit mass versions of (8) up to a difference term that decays like $O\left(\delta^2 \exp\left(-r_{ij}^2/\delta^2\right)\right)$, $O\left(\exp\left(-r_{ij}^2/\delta^2\right)\right)$, and $O\left(\left(1/\delta^2\right)\exp\left(-r_{ij}^2/\delta^2\right)\right)$ as $\delta \to 0$ when $m = 2, 4, 6$ respectively.

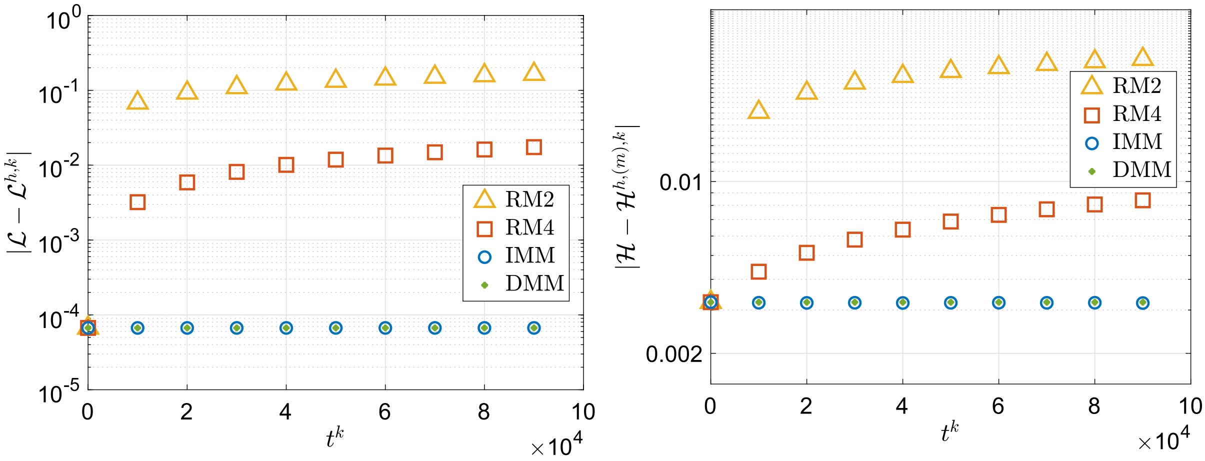

Fig. 4.4. Long-term behavior of $|\mathcal{L}^{h,N} - \mathcal{L}|$ (left) and $|\mathcal{H}^{h,(m),N} - \mathcal{H}|$ (right) when (13) is solved with $m = 4$, $T = 10^5$, and $\tau = 1.0$ using RM2, RM4, IMM, and DMM. The stars/circles/squares/triangles represent the error between the conserved integral and conserved quantity at $t^k \in \{1,\ 3,\ 10,\ 3\times 10^1,\ 1\times 10^2,\ 3\times 10^2,\ 1\times 10^3,\ 3\times 10^3,\ 1\times 10^4,\ 3\times 10^4,\ 1\times 10^5\}$.

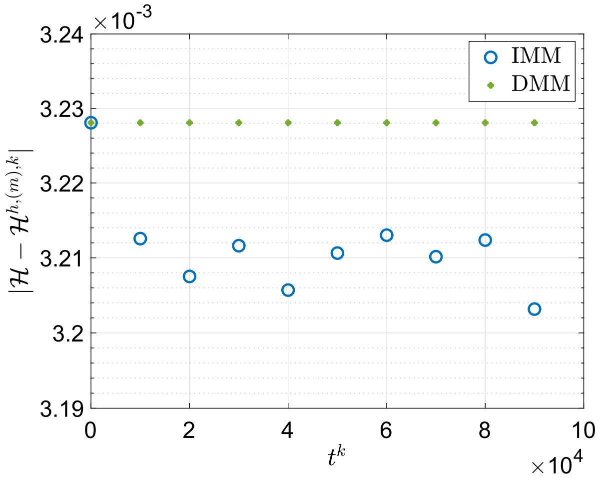

Fig. 4.5. Long-term behavior of $|\mathcal{H}^{h,(m),N} - \mathcal{H}|$ (right) when (13) is solved with $m = 4$, $T = 10^5$, and $\tau = 1.0$ using IMM and DMM. The stars/circles/squares/triangles represent the error between the conserved integral and conserved quantity at $t^k \in \{1,\ 3,\ 10,\ 3\times 10^1,\ 1\times 10^2,\ 3\times 10^2,\ 1\times 10^3,\ 3\times 10^3,\ 1\times 10^4,\ 3\times 10^4,\ 1\times 10^5\}$.

According to (26), the angular momentum error $|\mathcal{L}^{h,N} - \mathcal{L}|$ and the Hamiltonian error $|\mathcal{H}^{h,(m),N} - \mathcal{H}|$ should be of second order as $h \to 0$. While we see from Fig. 4.3 that the slope of the DMM curve in the $|\mathcal{H}^{h,(m),N} - \mathcal{H}|$ versus h plot is around two as expected, we see that its slope in the $|\mathcal{L}^{h,N} - \mathcal{L}|$ versus h plot exceeds two. Such superconvergence in the angular momentum error when using midpoint quadrature is attributed to the Laplacian of the integrand vanishing at $r = 1$. In general, we expect the angular momentum error to be of second order, similarly to the Hamiltonian error.

4.1.2. Long-term behavior of the error between conserved integrals and discretized conserved quantities

In a realistic fluid simulation, we also want the error between the conserved integrals of (3a)–(3e) and conserved quantities of (13) to remain bounded for all time. Otherwise, our numerical approximation will become less relevant physically as time proceeds. We show numerically below that this is true when (13) is solved via DMM-based integrators in (23).

Fig. 4.4 shows that the error between $\mathcal{L}$ and $\mathcal{L}^{h,k}$ grows with time when (13) is solved via RM2 or RM4. We see that the error between $\mathcal{H}$ and $\mathcal{H}^{h,(m),k}$ also grows with time when (13) is solved via RM2 and RM4. In Fig. 4.5 we see that, though the error $|\mathcal{H}^{h,(m),N} - \mathcal{H}|$ does not grow in time when (13) is solved via IMM, we can see that it fluctuates with time. In contrast, only the DMM methods yield in a numerical solution with almost constant $|\mathcal{L} - \mathcal{L}^{h,k}|$ and $|\mathcal{H} - \mathcal{H}^{h,(m),k}|$.

4.2. Comparison of vortex trajectories

We will now show that the long-term numerical solution of (3a)–(3e) obtained through DMM is qualitatively closer to the exact solution of (3a)–(3e) than the numerical solutions obtained through IMM, RM2, and RM4.

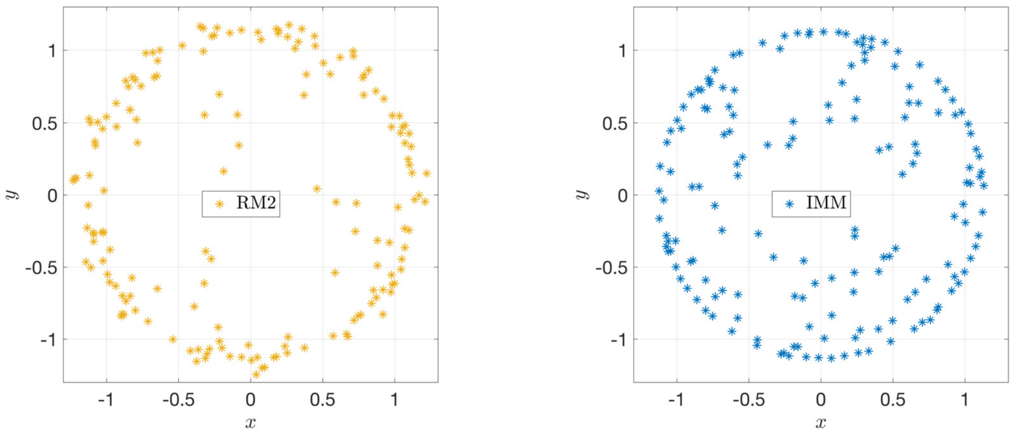

Fig. 4.6. Numerical path of a single vortex which is initially located at $(-1+h/2, -1+h/2)$ when (13) is solved via RM2 (left), IMM (right) with $T = 1650$ s, $\tau = 1.0$ and $M = 25$. Stars show the position of the vortex every 10 s.

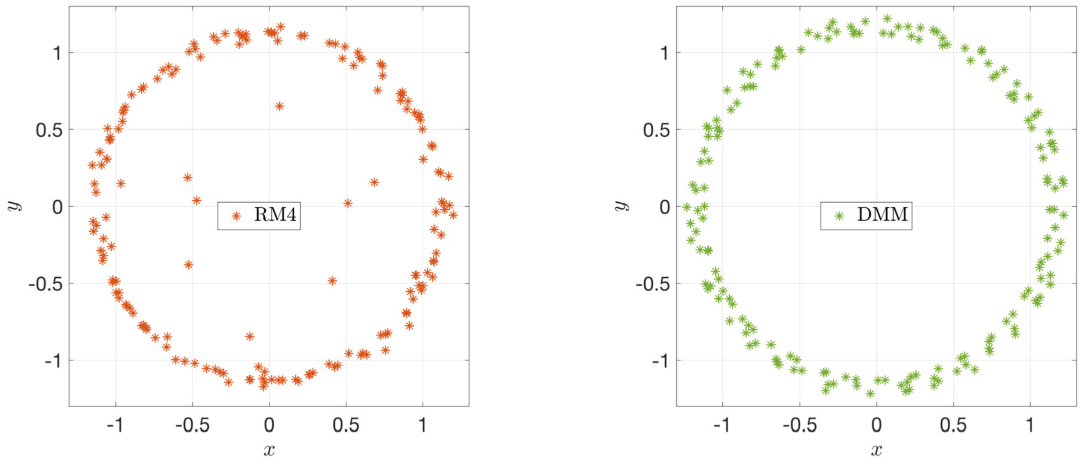

Fig. 4.7. Numerical path of a single vortex which is initially located at $(-1+h/2, -1+h/2)$ when (13) is solved via RM4 (left) and DMM (right) with $T = 1650$ s, $\tau = 1.0$ and $M = 25$. Stars show the position of the vortex every 10 s.

Figs. 4.6 and 4.7 illustrate the long-term ($T = 1650$) trajectory of the vortices initially placed at the center of leftmost, bottommost square (i.e., at $(-1+h/2, -1+h/2)$). It can be observed that trajectories produced by the 2^{nd} order integrators RM2 and IMM, and even a 4^{th} order integrator RM4, spiral toward the origin while the numerical trajectory produced by DMM stays close to the exact trajectory, which is a circle centered at the origin with radius $(1-h/2)\sqrt{2}$ as discussed earlier in (25). Note that the points on the interior of the disk occur only at later times.

4.3. Comparison of theoretical and numerical temporal convergence

Next, we verify numerically that the conservative schemes in (7) are 2^{nd} order accurate in time. In our convergence study we define the error between the exact solution and the numerical solution of (13) at time T to be,

$$\varepsilon_\tau = \left\| \begin{bmatrix} \boldsymbol{x}^M - \boldsymbol{x}(T) \\ \boldsymbol{y}^M - \boldsymbol{y}(T) \end{bmatrix} \right\|_2 . \tag{27}$$

To be able to evaluate ε_τ we need to have the exact solution of (13) at time T, that is $(\boldsymbol{x}(T), \boldsymbol{y}(T))$. For $N = 4$ and ω_0 is given by (24), the exact solution at time T is given by,

$$x_i(T) = R\cos(\alpha T + i\pi/2 - \pi/4), \quad y_i(T) = R\sin(\alpha T + +i\pi/2 - \pi/4), \quad \text{for} \quad i = 1, \ldots, N,$$

where $R = 1/\sqrt{2}$ and $\alpha = [C^{(m)}(1) + C^{(m)}(2)/2]/(8\pi)$. Fig. 4.8 shows that the error between DMM solution and the exact solution of (13) at time T is $O(\tau^2)$, which agrees with the conclusion of Theorem (3).

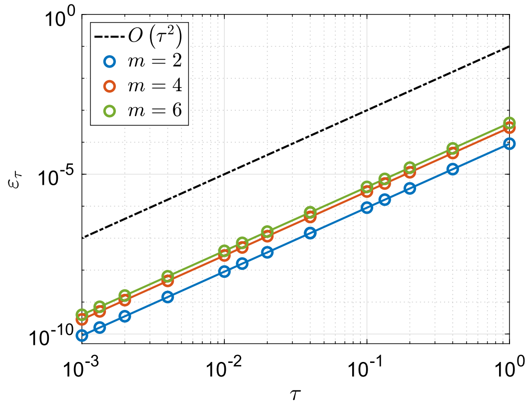

Fig. 4.8. Convergence of error (ε_τ) to zero as the time step size (τ) decreases when (13) is solved via (23) with $m = 2, 4, 6$, $T = 10.0$, and $M = 4$. Each circle of a given color (i.e., m) represents a point $(\tau^*, \varepsilon_\tau^*)$ in the convergence curve that was generated by implementing (23) with $\tau = \tau^*$. Each colored solid line is the best-fit line passing through the points illustrated by the circles of the same color. The dashed black line has a slope of 2 for reference.

Table 4.1
Theoretical [13] and computed spatial convergence orders for vortex blob methods with $m = 1, 2, 3$.

$T = 0.001$, $\tau = 0.001$, $q = 0.75$	$m = 2$	$m = 4$	$m = 6$
Theoretical order	1.50	3.00	4.50
Computed order	1.50	2.96	4.44[5]

4.4. Comparison of theoretical and numerical spatial convergence

In this subsection, we will show that the numerical solution of the PDE (3a)–(3e) obtained via the conservative discretizations (23) with $m = 2, 4, 6$ converges to the exact solution of (3a)–(3e) with the expected rate of convergence as $h \to 0$. We define the spatial discretization error between the numerical solution $\boldsymbol{v}^h(\boldsymbol{z}, t)$ and the exact solution $\boldsymbol{v}(\boldsymbol{z}, t)$ of (3a)–(3e) at time T to be

$$\varepsilon_h = \sqrt{\iint\limits_{\Omega(T)} \left\| \boldsymbol{v}^h(\boldsymbol{z}, T) - \boldsymbol{v}(\boldsymbol{z}, T) \right\|_2^2 \, d\boldsymbol{z}}. \tag{28}$$

Here, we evaluate $\boldsymbol{v}^h(\boldsymbol{z}, t)$ using (10) after obtaining the final position of each vortex by solving (13) via the conservative schemes. Also, recall that the exact solution $\boldsymbol{v}(\boldsymbol{z}, t)$ to (3a)–(3e) is available from (25). We numerically approximate the double integral over $\Omega(T)$ in (28) via an 8^{th} order Gaussian quadrature in polar coordinates. We used 8^{th} order quadrature to ensure that the quadrature error does not dominate the spatial discretization error.

Both Fig. 4.9 and Table 4.1 show that the order of convergence values for vortex blob methods of all orders implemented using (23) are in good agreement with the theoretical order of convergence values reported by Beale and Majda in [13].

4.5. Comparison of error in conserved quantity versus computation times

In this final subsection of numerical results, we will compare the computational time taken by the conservative integrators obtained via DMM to the computational time taken by the aforementioned standard integrators. To this end, we integrate (13) with $m = 2$ and $N = 3$ using DMM, IMM, RM2, and RM4. We set up five different vortex blob problems by randomly sampling ω_i of the vortices from a uniform distribution on $[-1, 1]$ and their initial positions from a uniform distribution on $[-1, 1] \times [-1, 1]$. We measure the computation time (wall-clock time) of all methods through the clock_gettime(CLOCK_REALTIME, &) function in time.h C library. The tables below summarize the computation time, as well as their maximum absolute errors in each conserved quantity, for each method on five different sample runs. In Table 4.2, we fix the number of time steps N when solving each problem, while on Table 4.3, we approximately fix the computational time by varying N for each method when solving the same problems in Table 4.2.

The purpose of the first table is to show that the conservative scheme preserves angular momentum, and in particular Hamiltonian, much better than the standard integrators when all methods are evaluated on the same number of time

[5] The spatial order of convergence when $m = 6$ was computed using a different ω_0 than the one we set in (24). We changed the exponent in ω_0 given in (24) from 3 to 15 because for convergence theory in [18] to hold when $m = 6, 8$ with the predicted order, ω_0 needs to have 14 bounded derivatives.

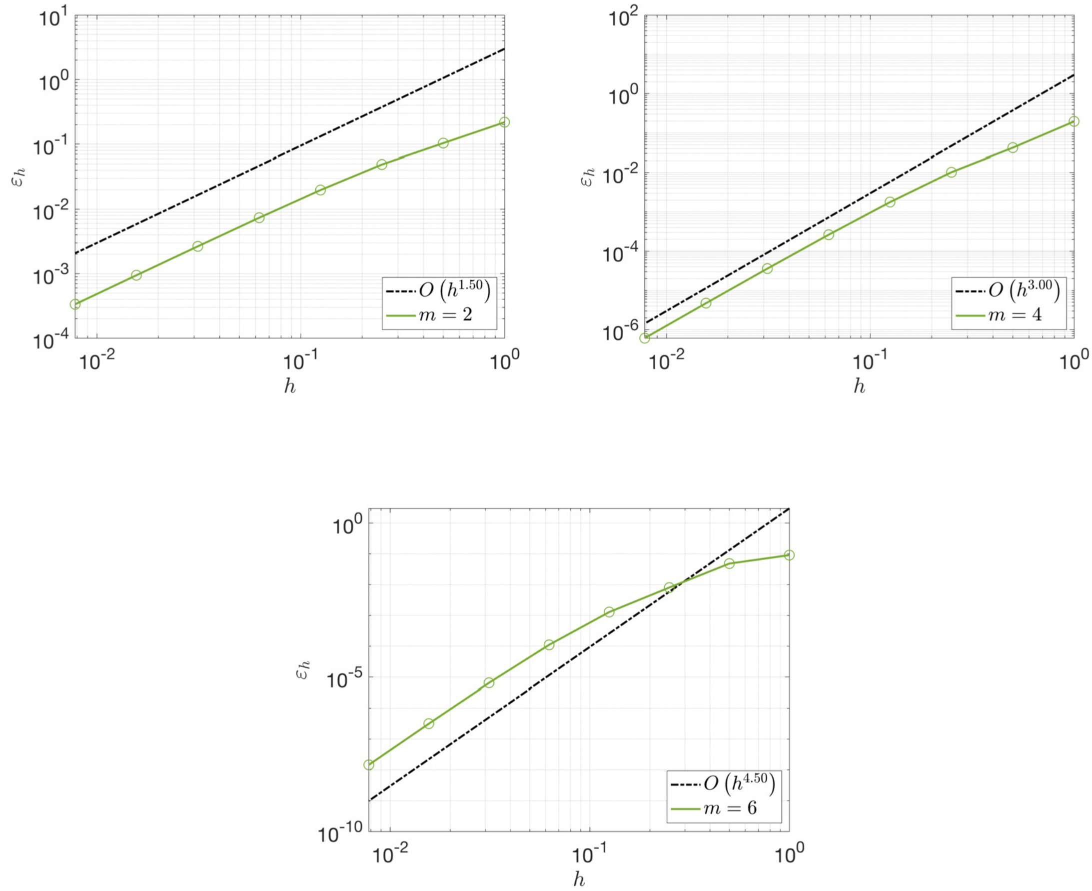

Fig. 4.9. Convergence of spatial error (ε_s) to zero as the grid size (h) decreases when (13) is solved via (23) with $m = 2, 4, 6$ and $T = 0.001$. Each circle is a point on the convergence curve.

Table 4.2
Computation times for solving (13) using RM2, RM4, IMM, and DMM discretizations with $T = 5 \times 10^6$, $M = 3$, $m = 2$, $\tau = 5.0$, $q = 0.75$. Each group of rows separated by double lines correspond to a specific sample run where $\omega_i, [\boldsymbol{x}_0]_i, [\boldsymbol{y}_0]_i \sim \mathcal{U}[-1, 1]$ for $i = 1, \dots, M$.

Method	# of time steps	Computation time [s]	Impulse-X	Impulse-Y	Angular impulse	Hamiltonian
DMM	10^6	149.09	3.8272×10^{-17}	5.5565×10^{-17}	2.0957×10^{-10}	3.8861×10^{-11}
IMM	10^6	28.05	4.7434×10^{-17}	8.1749×10^{-17}	3.8307×10^{-10}	1.1394×10^{-04}
RM2	10^6	1.73	1.5959×10^{-16}	1.6062×10^{-16}	2.2847×10^{00}	6.3812×10^{-02}
RM4	10^6	3.19	3.0358×10^{-18}	1.1926×10^{-18}	4.2929×10^{-01}	5.6505×10^{-02}
DMM	10^6	41.39	3.8856×10^{-15}	1.9076×10^{-15}	6.0627×10^{-12}	4.2839×10^{-14}
IMM	10^6	10.68	1.2423×10^{-15}	2.6096×10^{-15}	5.7927×10^{-12}	1.7762×10^{-05}
RM2	10^6	1.74	2.2207×10^{-15}	1.5642×10^{-15}	2.0692×10^{00}	4.5471×10^{-02}
RM4	10^6	3.30	1.6378×10^{-15}	1.1941×10^{-15}	3.8516×10^{-02}	2.1360×10^{-03}
DMM	10^6	39.27	7.0039×10^{-17}	1.2804×10^{-16}	4.2695×10^{-11}	6.5601×10^{-13}
IMM	10^6	9.70	7.4593×10^{-17}	1.7228×10^{-16}	1.1041×10^{-11}	1.0544×10^{-04}
RM2	10^6	1.74	4.7271×10^{-17}	1.0072×10^{-16}	2.2258×10^{-01}	1.6727×10^{-02}
RM4	10^6	3.24	8.7983×10^{-17}	2.1034×10^{-17}	4.8051×10^{-01}	2.6559×10^{-02}
DMM	10^6	38.02	1.8819×10^{-16}	4.2071×10^{-16}	3.9093×10^{-12}	1.3834×10^{-14}
IMM	10^6	6.92	1.9037×10^{-16}	7.3150×10^{-17}	4.0975×10^{-13}	4.1658×10^{-08}
RM2	10^6	1.55	3.7050×10^{-16}	1.8448×10^{-16}	4.1857×10^{-03}	1.5755×10^{-05}
RM4	10^6	2.95	2.5026×10^{-16}	2.9584×10^{-16}	4.2959×10^{-07}	1.4752×10^{-09}
DMM	10^6	49.87	5.4183×10^{-17}	2.1955×10^{-17}	2.7487×10^{-12}	3.6479×10^{-13}
IMM	10^6	11.58	2.5018×10^{-17}	3.5399×10^{-17}	2.6657×10^{-12}	2.6121×10^{-05}
RM2	10^6	1.73	5.1364×10^{-17}	9.6169×10^{-17}	2.1793×10^{00}	4.0292×10^{-02}
RM4	10^6	3.11	2.4259×10^{-17}	2.6536×10^{-17}	2.7556×10^{-01}	1.8089×10^{-02}

Table 4.3
Computation times for solving (13) using RM2, RM4, IMM, and DMM discretization with $T = 5 \times 10^6$, $M = 3$, $m = 2$, $q = 0.75$. Each group of rows separated by double lines correspond to a specific problem where $\omega_i, [\boldsymbol{x}_0]_i, [\boldsymbol{y}_0]_i \sim \mathcal{U}[-1, 1]$ for $i = 1, \ldots, M$.

Method	# of time steps	Computation time [s]	Impulse-X	Impulse-Y	Angular impulse	Hamiltonian
DMM	10^6	149.09	3.8272×10^{-17}	5.5565×10^{-17}	2.0957×10^{-10}	3.8861×10^{-11}
IMM	17×10^6	148.73	1.4680×10^{-16}	1.0045×10^{-16}	3.0382×10^{-10}	4.7884×10^{-07}
RM2	80×10^6	145.53	4.4062×10^{-16}	1.6279×10^{-16}	9.8936×10^{-03}	2.9922×10^{-03}
RM4	43×10^6	145.06	2.4698×10^{-16}	8.8559×10^{-17}	2.9535×10^{-06}	7.3229×10^{-07}
DMM	10^6	41.39	3.8856×10^{-15}	1.9076×10^{-15}	6.0627×10^{-12}	4.2839×10^{-14}
IMM	5×10^6	40.23	2.4839×10^{-15}	5.4754×10^{-15}	6.0298×10^{-12}	7.1217×10^{-07}
RM2	25×10^6	43.91	5.2460×10^{-15}	2.1628×10^{-14}	8.1034×10^{-04}	3.2301×10^{-05}
RM4	13×10^6	41.71	8.8885×10^{-15}	1.0839×10^{-14}	8.9068×10^{-08}	5.1731×10^{-09}
DMM	10^6	39.27	7.0039×10^{-17}	1.2804×10^{-16}	4.2695×10^{-11}	6.5601×10^{-13}
IMM	6×10^6	43.98	2.8796×10^{-16}	2.1760×10^{-16}	3.0895×10^{-12}	2.9561×10^{-06}
RM2	25×10^6	42.06	4.3043×10^{-16}	8.3397×10^{-16}	2.2287×10^{-03}	2.1921×10^{-04}
RM4	12×10^6	39.75	6.6722×10^{-16}	5.3484×10^{-16}	2.4074×10^{-06}	2.7789×10^{-07}
DMM	10^6	38.02	1.8819×10^{-16}	4.2071×10^{-16}	3.9093×10^{-12}	1.3834×10^{-14}
IMM	7×10^6	38.60	5.9208×10^{-16}	4.1873×10^{-16}	8.3213×10^{-13}	8.5027×10^{-10}
RM2	24×10^6	39.57	9.1812×10^{-16}	1.9575×10^{-15}	3.0487×10^{-07}	1.1382×10^{-09}
RM4	12×10^6	37.45	4.5671×10^{-16}	1.1610×10^{-15}	1.7587×10^{-12}	6.0769×10^{-15}
DMM	10^6	49.87	5.4183×10^{-17}	2.1955×10^{-17}	2.7487×10^{-12}	3.6479×10^{-13}
IMM	7×10^6	51.52	6.1122×10^{-17}	9.8012×10^{-17}	2.0447×10^{-11}	5.2790×10^{-07}
RM2	30×10^6	51.59	8.5896×10^{-17}	6.1583×10^{-17}	5.0931×10^{-03}	1.7794×10^{-04}
RM4	16×10^6	51.50	1.0010×10^{-16}	3.1106×10^{-16}	5.4385×10^{-07}	1.0184×10^{-10}

steps. The purpose of the second table is to show that, although the implicit conservative integrator is slower than the standard explicit integrators, it still preserves angular momentum and Hamiltonian better than standard integrators when all integrators are allowed to take similar computation times.

Specifically, we see from Table 4.2 that the DMM and IMM integrators preserve angular momentum on average about ten orders of magnitude better than RM2 and RM4. Moreover, we see that the DMM integrator preserves Hamiltonian on average about eight orders of magnitude better than IMM, ten order of magnitude better than RM2, and nine orders of magnitude better than RM4. The computational cost of such excellent conservative properties is about an increase of one to two orders of magnitude on average over the explicit schemes. Indeed, we can observe that DMM takes the longest while IMM takes the second longest amount in computation time, as both integrators are implicit schemes. However, compared to the overall improvement of eight to ten orders of magnitude in conserved quantities, this suggests that the derived DMM scheme can be suitable for applications where high-accuracy in conserved quantities is sought after.

We see that the conservation errors in angular-impulse for IMM and DMM are sometimes far from machine precision. This is due to the lack of convergence of the fixed-point iterations resulting from the poor conditioning of the nonlinear equations arising in IMM and DMM. When the vortex trajectories quickly depart from the unit-square in space, the nonlinear equation within the IMM and DMM schemes become ill-conditioned. Furthermore, the error in the conserved quantities is made worse for the angular-impulse due to its quadratic growth with respect to the position variables. We conducted numerical experiments in which we normalize the initial conditions by a fixed factor so that the vortices stay within the unit-square for all $t \in [0, T]$. With this modification, IMM and DMM were both able to preserve angular-impulse and Hamiltonian up to 10^{-15}.

Finally in Table 4.3, we see that the DMM and IMM integrators preserve angular momentum on average about eight orders of magnitude better than RM2 and RM4, when all methods are adjusted to take the same amount of computation time but different number of total time steps. In this comparison, we observed that DMM preserves the Hamiltonian on average about five orders of magnitude better than IMM, eight orders of magnitude better than RM2, and three orders of magnitude better than RM4. We note that, on the fourth sample run, we did observe that RM4 preserves the Hamiltonian slightly better than DMM while preserving the angular momentum equally well. We believe this is rare in practice, as this was the only instance of RM4 preserving Hamiltonian slightly better than DMM. Moreover, we attribute this to the frequent nonconvergence of fixed-point iterations resulting from the poor conditioning of the nonlinear equations. When we modified the initial positions as mentioned above, we observed that DMM preserved angular-impulse and Hamiltonian better than other methods in all test cases.

5. Conclusion

In this paper, we extended the work done on the point vortex method in [1] to obtain conservative integrators for higher-order vortex blob methods on the plane. While it is well known that point vortex methods have poorer accuracy when compared to vortex blob methods, we face two main difficulties when applying DMM to vortex blob method. First was evaluating the exponential integral term in the derived integrators and the second was the resulting DMM scheme being more complicated. We verified the conservation property of the derived integrators along with their order of convergence. Specifically, we verified the spatial order of convergence of higher-order vortex methods in [13] when the vortex blob equations were integrated through DMM. We also compared the derived integrators for the vortex blob equations to other classical integrators such as implicit midpoint and Ralston's 4th order method in terms of computational time versus error in conserved quantities. We observed that, for the vortex blob system with $m = 2$ and an initial configuration of randomly positioned vortices in $[-1, 1] \times [-1, 1]$ each having a uniform random vortex strength in $[-1, 1]$, the DMM integrator preserves the Hamiltonian many orders of magnitude better than a 4th order standard integrator and a 2nd order symplectic integrator when they take the same number of time steps. However, this conservation property came with two main costs. First, the process of computing the multiplier matrix and the scheme was nontrivial, and could be labor intensive for more complex systems. Second, the computational time taken per time step by our integrator was large compared to other integrators. When we compared our integrator to other integrators on comparable total computational time, we saw that our integrator still preserved Hamiltonian, on average, four orders of magnitude better than a 4th order standard integrator and six orders of magnitude better than a 2nd order symplectic integrator.

In principle, the work presented here can be adapted to other general vortex methods with more accurate and sophisticated interaction kernels, such as those given in [25] and [29]. Similarly, our work could be extended to have conservative vortex methods for 3D flows, or flows on the surface of a sphere, which might be of particular interest to climate modelers.

We conclude with a brief discussion on current limitations and future research directions. Specifically, the derived conservative discretizations currently have two main drawbacks. The first drawback is the fixed point iterations can have slow convergence and we observed that the convergence rate worsens as the number of vortices increases. Overcoming this drawback via the use of another nonlinear solver such as Newton or quasi-Newton methods is an interesting future research direction. A second drawback is associated with the fact that it takes $O\left(M^2\right)$ evaluations of the summands in (23). Overcoming this inefficiency is much more involved, yet may be possible through the use of fast multipole method (FMM) [37,38] introduced by Rokhlin and Greengard. We believe that combining DMM with fast multipole methods for many body problems is an important and fruitful future avenue for exploration, especially the number of bodies tend to be large for practical applications.

CRediT authorship contribution statement

Cem Gormezano: Methodology, Investigation, Code-Development, Visualization, Writing-Original Draft Preparation.
Jean-Christophe Nave: Supervision, Literature Review, Methodology, Writing-Reviewing and Editing.
Andy T.S. Wan: Supervision, Literature Review, Methodology, Writing-Reviewing and Editing.

Declaration of competing interest

The authors declare that they have no known competing financial interests or personal relationships that could have appeared to influence the work reported in this paper.

Acknowledgements

CG would like to acknowledge support from the ISM scholarship program and thank Paul Muir of Saint Mary's University for his comments on comparing numerical results with Ralston's methods. JCN acknowledges partial support from the NSERC Discovery Grant program (RGPIN-2019-0728). ATSW was partially supported by funding from the NSERC Discovery Grant program.

Appendix A

A.1. *Verification that condition (17b) holds*

$$\Lambda\left(\boldsymbol{x}, \boldsymbol{y}\right) \boldsymbol{f}\left(\boldsymbol{x}, \boldsymbol{y}\right)$$

$$
= \begin{pmatrix}
\frac{h^4}{2\pi}\sum_{i=1}^{M}\sum_{\substack{j=1\\ j\neq i}}^{M}\omega_i\omega_j x_{ij}\frac{C_{ij}^{(m)}}{r_{ij}^2} \\
\frac{h^4}{2\pi}\sum_{i=1}^{M}\sum_{\substack{j=1\\ j\neq i}}^{M}\omega_i\omega_j y_{ij}\frac{C_{ij}^{(m)}}{r_{ij}^2} \\
\frac{h^4}{2\pi}\sum_{i=1}^{M}\sum_{\substack{j=1\\ j\neq i}}^{M}\omega_i\omega_j\left(y_{ij}x_i - x_{ij}y_i\right)\frac{C_{ij}^{(m)}}{r_{ij}^2} \\
\frac{h^6}{4\pi^2}\sum_{i=1}^{M}\omega_i\sum_{\substack{l=1\\ l\neq i}}^{M}\sum_{\substack{j=1\\ j\neq i}}^{M}\omega_j\omega_l\left(x_{ij}y_{il}\frac{C_{ij}^{(m)}}{r_{ij}^2}\frac{C_{il}^{(m)}}{r_{il}^2} - y_{ij}x_{il}\frac{C_{ij}^{(m)}}{r_{ij}^2}\frac{C_{il}^{(m)}}{r_{il}^2}\right)
\end{pmatrix}
$$

$$
= \begin{pmatrix}
\frac{h^4}{2\pi}\sum_{1\le i<j\le M}\omega_i\omega_j\left(x_{ij}\frac{C_{ij}^{(m)}}{r_{ij}^2} + x_{ji}\frac{C_{ji}^{(m)}}{r_{ji}^2}\right) \\
\frac{h^4}{2\pi}\sum_{1\le i<j\le M}\omega_i\omega_j\left(y_{ij}\frac{C_{ij}^{(m)}}{r_{ij}^2} + y_{ji}\frac{C_{ji}^{(m)}}{r_{ji}^2}\right) \\
\frac{h^4}{2\pi}\sum_{1\le i<j\le M}\omega_i\omega_j\left[\left(y_{ij}x_i - x_{ij}y_i\right)\frac{C_{ij}^{(m)}}{r_{ij}^2} + \left(y_{ji}x_j - x_{ji}y_j\right)\frac{C_{ji}^{(m)}}{r_{ji}^2}\right] \\
\frac{h^6}{4\pi^2}\sum_{i=1}^{M}\omega_i\left[\sum_{\substack{l=1\\ l\neq i}}^{M}\sum_{\substack{j=1\\ j\neq i}}^{M}\omega_j\omega_l\left(y_{ij}x_{il}\frac{C_{ij}^{(m)}}{r_{ij}^2}\frac{C_{il}^{(m)}}{r_{il}^2}\right) - \sum_{\substack{l=1\\ l\neq i}}^{M}\sum_{\substack{j=1\\ j\neq i}}^{M}\omega_j\omega_l\left(x_{il}y_{ij}\frac{C_{ij}^{(m)}}{r_{ij}^2}\frac{C_{il}^{(m)}}{r_{il}^2}\right)\right]
\end{pmatrix}
$$

$$
= \mathbf{0},
$$

where,

$$
\begin{aligned}
r_{ij} &= r_{ji}, \\
C_{ij}^{(m)} &= C_{ji}^{(m)}, \\
x_{ij} &= -x_{ji}, \\
y_{ij} &= -y_{ji}, \\
y_{ij}x_i - x_{ij}y_i &= y_i x_j - y_j x_i = y_i x_j - y_j x_i + y_j x_j - y_j x_j = -\left(y_{ji}x_j - x_{ji}y_j\right).
\end{aligned}
$$

A.2. Verification that condition (22a) holds

Before we verify that condition (22a) is satisfied we give the following divided difference calculus identities.

(1) $\Delta\left(x_i^2 + y_i^2\right) = 2\overline{x_i}\Delta x_i + 2\overline{y_i}\Delta y_i$.

(2) $\Delta\left(r_{ij}^2\right) = 2\overline{x_{ij}}\Delta x_{ij} + 2\overline{y_{ij}}\Delta y_{ij}$.

(3) $\Delta\left(\log\left|r_{ij}^2\right|\right) = \log\left|r_{ij}^{k+1}\right|^2 - \log\left|r_{ij}^k\right|^2 = \log\left|\frac{r_{ij}^{k+1}}{r_{ij}^k}\right|^2 = \log\left|\frac{\xi_{ij}^{k+1}}{\xi_{ij}^k}\right|$.

(4) $\Delta\left(E_1\left[\left(\frac{r_{ij}}{\delta}\right)^2\right]\right) = E_1\left(\xi_{ij}^{k+1}\right) - E_1\left(\xi_{ij}^k\right)$.

(5) $\Delta\left(\exp\left[-\left(\frac{r_{ij}}{\delta}\right)^2\right]\right) = e^{-\xi_{ij}^k}\left(e^{-\Delta\xi_{ij}^k} - 1\right)$.

(6) Employing the discrete product rule and identity (5) we have,

$$
\Delta\left(\left(\frac{r_{ij}}{\delta}\right)^2\exp\left[-\left(\frac{r_{ij}}{\delta}\right)^2\right]\right) = e^{-\xi_{ij}^{k+1}}\Delta\xi_{ij} + \xi_{ij}^k\Delta\left(e^{-\xi_{ij}}\right)
$$

$$= e^{-\xi_{ij}^{k+1}}\Delta\xi_{ij} + \xi_{ij}^{k} e^{-\xi_{ij}^{k}}\left(e^{-\Delta\xi_{ij}} - 1\right).$$

(7) Employing the identities (3), (4) and (2) we have,

$$\Delta\left(\log\left|r_{ij}^2\right| + E_1\left[\left(\frac{r_{ij}}{\delta}\right)^2\right]\right)$$

$$= \left(\log\left|\frac{\xi_{ij}^{k+1}}{\xi_{ij}^{k}}\right| + E_1\left(\xi_{ij}^{k+1}\right) - E_1\left(\xi_{ij}^{k}\right)\right)\underbrace{\left(\frac{2\overline{x_{ij}}\Delta x_{ij} + 2\overline{y_{ij}}\Delta y_{ij}}{\Delta\left(r_{ij}^2\right)}\right)}_{=1}$$

$$= \left(\log\left|\frac{\xi_{ij}^{k+1}}{\xi_{ij}^{k}}\right| + E_1\left(\xi_{ij}^{k+1}\right) - E_1\left(\xi_{ij}^{k}\right)\right)\left(\frac{2\left(\overline{x_{ij}}\Delta x_{ij} + \overline{y_{ij}}\Delta y_{ij}\right)}{\left(r_{ij}^k\right)^2\left(\frac{\xi_{ij}^{k+1}}{\xi_{ij}^{k}} - 1\right)}\right)$$

$$= 2\left(\overline{x_{ij}}\Delta x_{ij} + \overline{y_{ij}}\Delta y_{ij}\right)\frac{C_{ij}^{\tau,(2)}}{\left(r_{ij}^k\right)^2}.$$

(8) Employing the identities (3), (4), (5), and (2) we have,

$$\Delta\left(\log\left|r_{ij}^2\right| + E_1\left[\left(\frac{r_{ij}}{\delta}\right)^2\right] - \exp\left[-\left(\frac{r_{ij}}{\delta}\right)^2\right]\right)$$

$$= \left(\log\left|\frac{\xi_{ij}^{k+1}}{\xi_{ij}^{k}}\right| + E_1\left(\xi_{ij}^{k+1}\right) - E_1\left(\xi_{ij}^{k}\right) - e^{-\xi_{ij}^{k}}\left(e^{-\Delta\xi_{ij}^{k}} - 1\right)\right)\left(\frac{2\left(\overline{x_{ij}}\Delta x_{ij} + \overline{y_{ij}}\Delta y_{ij}\right)}{\left(r_{ij}^k\right)^2\left(\frac{\xi_{ij}^{k+1}}{\xi_{ij}^{k}} - 1\right)}\right)$$

$$= 2\left(\overline{x_{ij}}\Delta x_{ij} + \overline{y_{ij}}\Delta y_{ij}\right)\frac{C_{ij}^{\tau,(4)}}{\left(r_{ij}^k\right)^2}.$$

(9) Employing the identities (3), (4), (5), (6) and (2) we have,

$$\Delta\left(\log\left|r_{ij}^2\right| + E_1\left[\left(\frac{r_{ij}}{\delta}\right)^2\right] + \left(-\frac{3}{2} + \frac{1}{2}\left(\frac{r_{ij}}{\delta}\right)^2\right)\exp\left[-\left(\frac{r_{ij}}{\delta}\right)^2\right]\right)$$

$$= \left(\log\left|\frac{\xi_{ij}^{k+1}}{\xi_{ij}^{k}}\right| + E_1\left(\xi_{ij}^{k+1}\right) - E_1\left(\xi_{ij}^{k}\right) + \Delta\left(e^{-\xi_{ij}}\right)\left(-\frac{3}{2} + \frac{1}{2}\xi_{ij}^{k}\right) + \frac{1}{2}e^{-\xi_{ij}^{k+1}}\Delta\xi_{ij}\right)\left(\frac{2\left(\overline{x_{ij}}\Delta x_{ij} + \overline{y_{ij}}\Delta y_{ij}\right)}{\left(r_{ij}^k\right)^2\left(\frac{\xi_{ij}^{k+1}}{\xi_{ij}^{k}} - 1\right)}\right)$$

$$= \frac{2\left(\overline{x_{ij}}\Delta x_{ij} + \overline{y_{ij}}\Delta y_{ij}\right)}{\left(r_{ij}^k\right)^2}\left[\frac{1}{\frac{\xi_{ij}^{k+1}}{\xi_{ij}^{k}} - 1}\left(\log\left|\frac{\xi_{ij}^{k+1}}{\xi_{ij}^{k}}\right| + E_1\left(\xi_{ij}^{k+1}\right) - E_1\left(\xi_{ij}^{k}\right) + \right.\right.$$

$$\Delta\left(e^{-\xi_{ij}}\right)\left(-\frac{3}{2}+\frac{1}{2}\xi_{ij}^{k}\right)\Bigg)+\frac{1}{2}\frac{e^{-\xi_{ij}^{k+1}}\Delta\xi_{ij}}{\frac{\xi_{ij}^{k+1}}{\xi_{ij}^{k}}-1}\Bigg]$$

$$= \frac{2\left(\overline{x_{ij}}\Delta x_{ij}+\overline{y_{ij}}\Delta y_{ij}\right)}{\left(r_{ij}^{k}\right)^{2}}\Bigg[\frac{1}{\frac{\xi_{ij}^{k+1}}{\xi_{ij}^{k}}-1}\Bigg(\log\left|\frac{\xi_{ij}^{k+1}}{\xi_{ij}^{k}}\right|+E_1\left(\xi_{ij}^{k+1}\right)-E_1\left(\xi_{ij}^{k}\right)+ e^{-\xi_{ij}^{k}}\left(e^{-\Delta\xi_{ij}^{k}}-1\right)\left(-\frac{3}{2}+\frac{1}{2}\xi_{ij}^{k}\right)\Bigg)+\frac{1}{2}\xi_{ij}^{k}e^{-\xi_{ij}^{k+1}}\Bigg]$$

$$= 2\left(\overline{x_{ij}}\Delta x_{ij}+\overline{y_{ij}}\Delta y_{ij}\right)\frac{C_{ij}^{\tau,(6)}}{\left(r_{ij}^{k}\right)^{2}}.$$

Then, condition (22a) is satisfied for $m = 2, 4, 6$ by the linearity of Δ operator and by the identities (1)–(9) because,

$$\Lambda^{\tau}D_t^{\tau}\boldsymbol{x} = \frac{1}{\tau}\begin{pmatrix} h^2\sum_{i=1}^{M}\omega_i\Delta y_i \\ -h^2\sum_{i=1}^{M}\omega_i\Delta x_i \\ -h^2\sum_{i=1}^{M}\omega_i\left(\overline{x_i}\Delta x_i+\overline{y_i}\Delta y_i\right) \\ -\frac{h^4}{2\pi}\sum_{i=1}^{M}\sum_{\substack{j=1\\ j\neq i}}^{M}\omega_i\omega_j\left(\overline{x_{ij}}\Delta x_i+\overline{y_{ij}}\Delta y_i\right)\frac{C_{ij}^{\tau,(m)}}{\left(r_{ij}^{k}\right)^{2}}\end{pmatrix}$$

$$= \frac{1}{\tau}\begin{pmatrix} \Delta\left(h^2\sum_{i=1}^{M}\omega_i y_i\right) \\ \Delta\left(-h^2\sum_{i=1}^{M}\omega_i x_i\right) \\ \Delta\left(-\frac{h^2}{2}\sum_{i=1}^{M}\omega_i\left(x_i^2+y_i^2\right)\right) \\ -\frac{h^4}{4\pi}\sum_{1\le i<j\le M}2\,\omega_i\omega_j\left(\overline{x_{ij}}\Delta x_i+\overline{y_{ij}}\Delta y_i+\overline{x_{ji}}\Delta x_j+\overline{y_{ji}}\Delta y_j\right)\frac{C_{ij}^{\tau,(m)}}{\left(r_{ij}^{k}\right)^{2}}\end{pmatrix}$$

$$= \frac{1}{\tau}\begin{pmatrix}\Delta\mathcal{P}\\ \Delta\mathcal{L}\\ \Delta\mathcal{H}^{(m),h}\end{pmatrix} = D_t^{\tau}\boldsymbol{\psi}-\partial_t^{\tau}\boldsymbol{\psi},$$

where the 3rd equality for the 4th row follows from,

$$\overline{x_{ij}}\Delta x_i+\overline{y_{ij}}\Delta y_i+\overline{x_{ji}}\Delta x_j+\overline{y_{ji}}\Delta y_j = \overline{x_{ij}}\Delta x_{ij}+\overline{y_{ij}}\Delta y_{ij}.$$

A.3. Verification that condition (22b) holds

$$\Lambda^{\tau}\boldsymbol{f}^{\tau}$$

$$= \begin{pmatrix} \frac{h^4}{2\pi}\sum_{i=1}^{M}\sum_{\substack{j=1\\ j\neq i}}^{M}\omega_i\omega_j\frac{\overline{x_{ij}}}{\left(r_{ij}^k\right)^2}C_{ij}^{\tau,(m)} \\ \frac{h^4}{2\pi}\sum_{i=1}^{M}\sum_{\substack{j=1\\ j\neq i}}^{M}\omega_i\omega_j\frac{\overline{y_{ij}}}{\left(r_{ij}^k\right)^2}C_{ij}^{\tau,(m)} \\ \frac{h^4}{2\pi}\sum_{i=1}^{M}\sum_{\substack{j=1\\ j\neq i}}^{M}\omega_i\omega_j\frac{\left(\overline{y_{ij}}\,\overline{x_i}-\overline{x_{ij}}\,\overline{y_i}\right)}{\left(r_{ij}^k\right)^2}C_{ij}^{\tau,(m)} \\ \frac{h^6}{4\pi^2}\sum_{i=1}^{M}\omega_i\sum_{\substack{l=1\\ l\neq i}}^{M}\sum_{\substack{j=1\\ j\neq i}}^{M}\omega_j\omega_l\left(\frac{\overline{x_{ij}}}{\left(r_{ij}^k\right)^2}\frac{\overline{y_{il}}}{\left(r_{il}^k\right)^2}C_{ij}^{\tau,(m)}C_{il}^{\tau,(m)}-\frac{\overline{y_{ij}}}{\left(r_{ij}^k\right)^2}\frac{\overline{x_{il}}}{\left(r_{il}^k\right)^2}C_{ij}^{\tau,(m)}C_{il}^{\tau,(m)}\right) \end{pmatrix}$$

$$= \begin{pmatrix} \frac{h^4}{2\pi}\sum_{1\le i<j\le M}\omega_i\omega_j\left(\frac{\overline{x_{ij}}}{\left(r_{ij}^k\right)^2}C_{ij}^{\tau,(m)}+\frac{\overline{x_{ji}}}{\left(r_{ji}^k\right)^2}C_{ji}^{\tau,(m)}\right) \\ \frac{h^4}{2\pi}\sum_{1\le i<j\le M}\omega_i\omega_j\left(\frac{\overline{y_{ij}}}{\left(r_{ij}^k\right)^2}C_{ij}^{\tau,(m)}+\frac{\overline{y_{ji}}}{\left(r_{ji}^k\right)^2}C_{ji}^{\tau,(m)}\right) \\ \frac{h^4}{2\pi}\sum_{1\le i<j\le M}\omega_i\omega_j\left(\frac{\left(\overline{y_{ij}}\,\overline{x_i}-\overline{x_{ij}}\,\overline{y_i}\right)}{\left(r_{ij}^k\right)^2}C_{ij}^{\tau,(m)}+\frac{\left(\overline{y_{ji}}\,\overline{x_j}-\overline{x_{ji}}\,\overline{y_j}\right)}{\left(r_{ji}^k\right)^2}C_{ji}^{\tau,(m)}\right) \\ \frac{h^6}{4\pi^2}\sum_{i=1}^{M}\omega_i\left[\sum_{\substack{l=1\\ l\neq i}}^{M}\sum_{\substack{j=1\\ j\neq i}}^{M}\omega_j\omega_l\left(\frac{\overline{y_{ij}}}{\left(r_{ij}^k\right)^2}\frac{\overline{x_{il}}}{\left(r_{il}^k\right)^2}C_{ij}^{\tau,(m)}C_{il}^{\tau,(m)}\right)-\sum_{\substack{l=1\\ l\neq i}}^{M}\sum_{\substack{j=1\\ j\neq i}}^{M}\omega_j\omega_l\left(\frac{\overline{x_{il}}}{\left(r_{il}^k\right)^2}\frac{\overline{y_{ij}}}{\left(r_{ij}^k\right)^2}C_{ij}^{\tau,(m)}C_{il}^{\tau,(m)}\right)\right] \end{pmatrix}$$

$$= \mathbf{0},$$

where the last equality follows from,

$$\begin{aligned} r_{ij}^k &= r_{ji}^k, \\ \xi_{ij}^k &= \xi_{ji}^k, \\ \overline{x_{ij}} &= -\overline{x_{ji}}, \\ \overline{y_{ij}} &= -\overline{y_{ji}}, \end{aligned}$$

$$\overline{y_{ij}}\,\overline{x_i}-\overline{x_{ij}}\,\overline{y_i}=\overline{y_i}\,\overline{x_j}-\overline{y_j}\,\overline{x_i}=\overline{y_i}\,\overline{x_j}-\overline{y_j}\,\overline{x_i}+\overline{y_j}\,\overline{x_j}-\overline{y_j}\,\overline{x_j}=-\left(\overline{y_{ji}}\,\overline{x_j}-\overline{x_{ji}}\,\overline{y_j}\right).$$

A.4. Proof that the conservative scheme (23) is symmetric

We define,

$$V_{ij}^{(2)} := V_{ij}^{(2)}\left(r_{ij}^2\right) = \log\left|r_{ij}^2\right| + E_1\left(\frac{r_{ij}^2}{\delta^2}\right),$$

$$V_{ij}^{(4)} := V_{ij}^{(4)}\left(r_{ij}^2\right) = \log\left|r_{ij}^2\right| + E_1\left(\frac{r_{ij}^2}{\delta^2}\right) - \exp\left(-\frac{r_{ij}^2}{\delta^2}\right),$$

$$V_{ij}^{(6)} := V_{ij}^{(6)}\left(r_{ij}^2\right) = \log\left|r_{ij}^2\right| + E_1\left(\frac{r_{ij}^2}{\delta^2}\right) + \left(-\frac{3}{2}+\frac{1}{2}\left(\frac{r_{ij}^2}{\delta^2}\right)\right)\exp\left(-\frac{r_{ij}^2}{\delta^2}\right).$$

Then, we can express (23) as,

$$\boldsymbol{F}^{\tau}\left(\boldsymbol{x}^{k+1},\boldsymbol{y}^{k+1},\boldsymbol{x}^{k},\boldsymbol{y}^{k}\right):=\left(\begin{array}{c}\left[\dfrac{x_i^{k+1}-x_i^k}{\tau}+\dfrac{h^2}{2\pi}\sum_{j=1,j\neq i}^{N}\omega_j\overline{y_{ij}}\,\dfrac{\Delta V_{ij}^{(m)}}{\Delta\left(r_{ij}^2\right)}\right]_{1\le i\le N}\\ \left[\dfrac{y_i^{k+1}-y_i^k}{\tau}-\dfrac{h^2}{2\pi}\sum_{j=1,j\neq i}^{N}\omega_j\overline{x_{ij}}\,\dfrac{\Delta V_{ij}^{(m)}}{\Delta\left(r_{ij}^2\right)}\right]_{1\le i\le N}\end{array}\right)=\boldsymbol{0}.$$

Due to their definitions, $\overline{x_{ij}}$, $\overline{y_{ij}}$, and $\Delta V_{ij}^{(m)}/\Delta\left(r_{ij}^2\right)$ are all symmetric under the permutation $k\leftrightarrow k+1$. Thus, (23) is symmetric under the permutation $k\leftrightarrow k+1$.

A.5. Derivation of Taylor series expansions of $C_{ij}^{\tau,(2)}$, $C_{ij}^{\tau,(4)}$, and $C_{ij}^{\tau,(6)}$

A.5.1. $C_{ij}^{\tau,(2)}$

Using the Taylor series expansion of the exponential integral $E_1(x)=-\gamma-\log|x|-\sum_{l=1}^{\infty}\frac{(-x)^l}{l.l!}$ in [33] where γ is the Euler–Mascheroni constant, and letting $z_{ij}=\xi_{ij}^{k+1}/\xi_{ij}^{k}$ we have,

$$\begin{aligned}
C_{ij}^{\tau,(2)}&=\frac{1}{\dfrac{\xi_{ij}^{k+1}}{\xi_{ij}^{k}}-1}\left[\log\left|\frac{\xi_{ij}^{k+1}}{\xi_{ij}^{k}}\right|+E_1\left(\xi_{ij}^{k+1}\right)-E_1\left(\xi_{ij}^{k}\right)\right]\\
&=\frac{1}{z_{ij}-1}\left[\log\left|z_{ij}\right|+E_1\left(z_{ij}\xi_{ij}^{k}\right)-E_1\left(\xi_{ij}^{k}\right)\right]\\
&=\frac{1}{z_{ij}-1}\left[\log\left|z_{ij}\right|-\log\left|z_{ij}\xi_{ij}^{k}\right|-\sum_{l=1}^{\infty}\frac{\left(-z_{ij}\xi_{ij}^{k}\right)^l}{l.l!}+\log\left|\xi_{ij}^{k}\right|+\sum_{l=1}^{\infty}\frac{\left(-\xi_{ij}^{k}\right)^l}{l.l!}\right]\\
&=-\frac{1}{z_{ij}-1}\left[\sum_{l=1}^{\infty}\frac{\left(-\xi_{ij}^{k}\right)^l}{l.l!}\left(\left(z_{ij}\right)^l-1\right)\right]\\
&=-\sum_{l=1}^{\infty}\frac{\left(-\xi_{ij}^{k}\right)^l}{l.l!}\left(\sum_{m=0}^{l-1}\left(z_{ij}\right)^m\right)\\
&=-\sum_{l=1}^{\infty}\frac{\left(-\xi_{ij}^{k}\right)^l}{l.l!}\left(\sum_{m=0}^{l-1}\left(z_{ij}-1+1\right)^m\right)\\
&=-\sum_{l=1}^{\infty}\frac{\left(-\xi_{ij}^{k}\right)^l}{l.l!}\left(\sum_{m=0}^{l-1}\sum_{n=0}^{m}\frac{m!}{n!\,(m-n)!}\left(z_{ij}-1\right)^n\right)\\
&=-\sum_{l=1}^{\infty}\frac{\left(-\xi_{ij}^{k}\right)^l}{l.l!}\left[\sum_{m=0}^{l-1}\left(1+m\left(z_{ij}-1\right)+\frac{m\,(m-1)}{2}\left(z_{ij}-1\right)^2+\dots+\left(z_{ij}-1\right)^m\right)\right].
\end{aligned}$$

By keeping the 2$^{\text{nd}}$ order terms we obtain,

$$C_{ij}^{\tau,(2)}=-\sum_{l=1}^{\infty}\frac{\left(-\xi_{ij}^{k}\right)^l}{l.l!}\left[\sum_{m=0}^{l-1}1+\left(z_{ij}-1\right)\sum_{m=0}^{l-1}m+\left(z_{ij}-1\right)^2\sum_{m=0}^{l-1}\frac{m\,(m-1)}{2}+\dots\right].$$

Using the summation identities $\sum_{m=1}^{l}m=\frac{l\,(l+1)}{2}$ and $\sum_{m=1}^{l}m^2=\frac{l\,(l+1)\,(2l+1)}{6}$, we get,

$$C_{ij}^{\tau,(2)} = -\sum_{l=1}^{\infty} \frac{\left(-\xi_{ij}^k\right)^l}{l!} - \frac{\left(z_{ij}-1\right)}{2} \sum_{l=1}^{\infty} \frac{\left(-\xi_{ij}^k\right)^l}{l!}(l-1) - \frac{\left(z_{ij}-1\right)^2}{6} \sum_{l=1}^{\infty} \frac{\left(-\xi_{ij}^k\right)^l}{l!}\left(l^2-3l+2\right) - \dots.$$

Finally using the Taylor series expansions, $\sum_{l=0}^{\infty} \frac{\left(-\xi_{ij}^k\right)^l}{l!} = e^{-\xi_{ij}^k}$, $\sum_{l=0}^{\infty} \frac{l\left(-\xi_{ij}^k\right)^l}{l!} = -\xi_{ij}^k e^{-\xi_{ij}^k}$, and $\sum_{l=0}^{\infty} \frac{l^2\left(-\xi_{ij}^k\right)^l}{l!} = e^{-\xi_{ij}^k}\left[-\xi_{ij}^k + \left(\xi_{ij}^k\right)^2\right]$ yields,

$$\boxed{C_{ij}^{\tau,(2)} = \left(1-e^{-\xi_{ij}^k}\right) + \frac{\left(z_{ij}-1\right)}{2}\left(-1+\left(1+\xi_{ij}^k\right)e^{-\xi_{ij}^k}\right) + \frac{\left(z_{ij}-1\right)^2}{6}\left(2+\left(-2-2\xi_{ij}^k-\left(\xi_{ij}^k\right)^2\right)e^{-\xi_{ij}^k}\right) + \dots.}$$

A.5.2. $C_{ij}^{\tau,(4)}$

We can represent $C_{ij}^{\tau,(4)}$ in terms of $C_{ij}^{\tau,(2)}$ such that,

$$\begin{aligned}
C_{ij}^{\tau,(4)} &= \frac{1}{\frac{\xi_{ij}^{k+1}}{\xi_{ij}^k}-1}\left[\log\left|\frac{\xi_{ij}^{k+1}}{\xi_{ij}^k}\right| + E_1\left(\xi_{ij}^{k+1}\right) - E_1\left(\xi_{ij}^k\right) - e^{-\xi_{ij}^k}\left(e^{-\Delta\xi_{ij}}-1\right)\right] \\
&= C_{ij}^{\tau,(2)} - \frac{1}{\frac{\xi_{ij}^{k+1}}{\xi_{ij}^k}-1}\left[e^{-\xi_{ij}^k}\left(e^{-\Delta\xi_{ij}}-1\right)\right] \\
&= C_{ij}^{\tau,(2)} - \frac{1}{z_{ij}-1}\left[e^{-\xi_{ij}^k}\left(e^{-\xi_{ij}^k\left(z_{ij}-1\right)}-1\right)\right].
\end{aligned}$$

Using the Taylor series expansion $e^{-\xi_{ij}^k\left(z_{ij}^k-1\right)} = \sum_{l=0}^{\infty} \frac{\left(-\xi_{ij}^k\left(z_{ij}-1\right)\right)^l}{l!}$ up to 3$^{\text{rd}}$ order we get,

$$\begin{aligned}
C_{ij}^{\tau,(4)} &= C_{ij}^{\tau,(2)} - \frac{1}{z_{ij}-1}\left[e^{-\xi_{ij}^k}\left(1-\left(z_{ij}-1\right)\xi_{ij}^k + \left(z_{ij}-1\right)^2\frac{\left(\xi_{ij}^k\right)^2}{2} - \left(z_{ij}-1\right)^3\frac{\left(\xi_{ij}^k\right)^3}{6} + \dots - 1\right)\right] \\
&= C_{ij}^{\tau,(2)} + \left(\xi_{ij}^k e^{-\xi_{ij}^k}\right) + \frac{\left(z_{ij}-1\right)}{2}\left(-\left(\xi_{ij}^k\right)^2 e^{-\xi_{ij}^k}\right) + \frac{\left(z_{ij}-1\right)^2}{6}\left(\left(\xi_{ij}^k\right)^3 e^{-\xi_{ij}^k}\right).
\end{aligned}$$

Finally we have,

$$\boxed{C_{ij}^{\tau,(4)} = \left(1+\left(-1+\xi_{ij}^k\right)e^{-\xi_{ij}^k}\right) + \frac{\left(z_{ij}-1\right)}{2}\left(-1+\left(1+\xi_{ij}^k-\left(\xi_{ij}^k\right)^2\right)e^{-\xi_{ij}^k}\right) + \frac{\left(z_{ij}-1\right)^2}{6}\left(2+\left(-2-2\xi_{ij}^k-\left(\xi_{ij}^k\right)^2+\left(\xi_{ij}^k\right)^3\right)e^{-\xi_{ij}^k}\right) + \dots.}$$

A.5.3. $C_{ij}^{\tau,(6)}$

Similar to $C_{ij}^{\tau,(4)}$, the form of $C_{ij}^{\tau,(6)}$ allows us to represent it in terms of $C_{ij}^{\tau,(2)}$ such that,

$$\begin{aligned} C_{ij}^{\tau,(6)} &= \frac{1}{\frac{\xi_{ij}^{k+1}}{\xi_{ij}^{k}}-1}\left[\log\left|\frac{\xi_{ij}^{k+1}}{\xi_{ij}^{k}}\right| + E_1\left(\xi_{ij}^{k+1}\right) - E_1\left(\xi_{ij}^{k}\right) + e^{-\xi_{ij}^{k}}\left(e^{-\Delta\xi_{ij}}-1\right)\left(-\frac{3}{2}+\frac{1}{2}\xi_{ij}^{k}\right)\right] + \frac{1}{2}\xi_{ij}^{k}e^{-\xi_{ij}^{k+1}} \\ &= C_{ij}^{\tau,(2)} + \frac{1}{\frac{\xi_{ij}^{k+1}}{\xi_{ij}^{k}}-1}\left[e^{-\xi_{ij}^{k}}\left(e^{-\Delta\xi_{ij}}-1\right)\left(-\frac{3}{2}+\frac{1}{2}\xi_{ij}^{k}\right)\right] + \frac{1}{2}\xi_{ij}^{k}e^{-\xi_{ij}^{k+1}} \\ &= C_{ij}^{\tau,(2)} + \frac{1}{z_{ij}-1}\left[e^{-\xi_{ij}^{k}}\left(e^{-\xi_{ij}^{k}(z_{ij}-1)}-1\right)\left(-\frac{3}{2}+\frac{1}{2}\xi_{ij}^{k}\right)\right] + \frac{1}{2}\left(\xi_{ij}^{k}e^{-\xi_{ij}^{k}}\right)e^{-\xi_{ij}^{k}(z_{ij}-1)}. \end{aligned}$$

As before, using the Taylor series expansion of $e^{-\xi_{ij}^{k}\left(z_{ij}^{k}-1\right)}$ we get,

$$\begin{aligned} C_{ij}^{\tau,(6)} &= C_{ij}^{\tau,(2)} + \frac{1}{z_{ij}-1}\left[e^{-\xi_{ij}^{k}}\left(1-\left(z_{ij}-1\right)\xi_{ij}^{k} + \left(z_{ij}-1\right)^2\frac{\left(\xi_{ij}^{k}\right)^2}{2} - \left(z_{ij}-1\right)^3\frac{\left(\xi_{ij}^{k}\right)^3}{6} + \cdots - 1\right)\left(-\frac{3}{2}+\frac{1}{2}\xi_{ij}^{k}\right)\right] + \\ &\qquad \frac{1}{2}\xi_{ij}^{k}e^{-\xi_{ij}^{k}}\left(1-\left(z_{ij}-1\right)\xi_{ij}^{k}+\left(z_{ij}-1\right)^2\frac{\left(\xi_{ij}^{k}\right)^2}{2}-\cdots\right) \\ &= C_{ij}^{\tau,(2)} + e^{-\xi_{ij}^{k}}\left(-\xi_{ij}^{k}+\left(z_{ij}-1\right)\frac{\left(\xi_{ij}^{k}\right)^2}{2}-\left(z_{ij}-1\right)^2\frac{\left(\xi_{ij}^{k}\right)^3}{6}+\cdots\right)\left(-\frac{3}{2}+\frac{1}{2}\xi_{ij}^{k}\right) + \\ &\qquad \frac{1}{2}\xi_{ij}^{k}e^{-\xi_{ij}^{k}}\left(1-\left(z_{ij}-1\right)\xi_{ij}^{k}+\left(z_{ij}-1\right)^2\frac{\left(\xi_{ij}^{k}\right)^2}{2}-\cdots\right) \\ &= C_{ij}^{\tau,(2)} + \left(2\xi_{ij}^{k}-\frac{1}{2}\left(\xi_{ij}^{k}\right)^2\right)e^{-\xi_{ij}^{k}} + \frac{\left(z_{ij}-1\right)}{2}\left(-\frac{5}{2}\left(\xi_{ij}^{k}\right)^2+\frac{1}{2}\left(\xi_{ij}^{k}\right)^3\right)e^{-\xi_{ij}^{k}} + \\ &\qquad \frac{\left(z_{ij}-1\right)^2}{6}\left(3\left(\xi_{ij}^{k}\right)^3-\frac{1}{2}\left(\xi_{ij}^{k}\right)^4\right)e^{-\xi_{ij}^{k}} + \cdots. \end{aligned}$$

Finally we have,

$$\boxed{\begin{aligned} C_{ij}^{\tau,(6)} = &\left(1+\left(-1+2\xi_{ij}^{k}-\frac{1}{2}\left(\xi_{ij}^{k}\right)^2\right)e^{-\xi_{ij}^{k}}\right) + \\ &\frac{\left(z_{ij}-1\right)}{2}\left(-1+\left(1+\xi_{ij}^{k}-\frac{5}{2}\left(\xi_{ij}^{k}\right)^2+\frac{1}{2}\left(\xi_{ij}^{k}\right)^3\right)e^{-\xi_{ij}^{k}}\right) + \\ &\frac{\left(z_{ij}-1\right)^2}{6}\left(2+\left(-2-2\xi_{ij}^{k}-\left(\xi_{ij}^{k}\right)^2+3\left(\xi_{ij}^{k}\right)^3-\frac{1}{2}\left(\xi_{ij}^{k}\right)^4\right)e^{-\xi_{ij}^{k}}\right) + \cdots. \end{aligned}}$$

A.5.4. Demonstrating the necessity of the Taylor series expansions of $C^{\tau,(2)}$, $C^{\tau,(4)}$, and $C^{\tau,(6)}$ due to round-off errors

Fig. A.1 shows that when $\tilde{C}_{ij}^{\tau,(m)}$ is set to be the 2nd order Taylor expansion of $C_{ij}^{\tau,(m)}$, the error between $\tilde{C}_{ij}^{\tau,(m)}$ and $C_{ij}^{\tau,(m)}$ converges to zero with 3rd-order accuracy until $z_{ij}-1\approx 10^{-4}$. After $z_{ij}-1\approx 10^{-4}$, we see that the error between $\tilde{C}_{ij}^{\tau,(m)}$ and $C_{ij}^{\tau,(m)}$ increase markedly due to round-off error emanating from the evaluation of $C_{ij}^{\tau,(m)}$. Thus, it is clear that we need to employ $\tilde{C}_{ij}^{\tau,(2)}$, $\tilde{C}_{ij}^{\tau,(4)}$, and $\tilde{C}_{ij}^{\tau,(6)}$ instead of $C_{ij}^{\tau(2)}$, $C_{ij}^{\tau,(4)}$, and $C_{ij}^{\tau,(6)}$ respectively for (23) to be conservative up

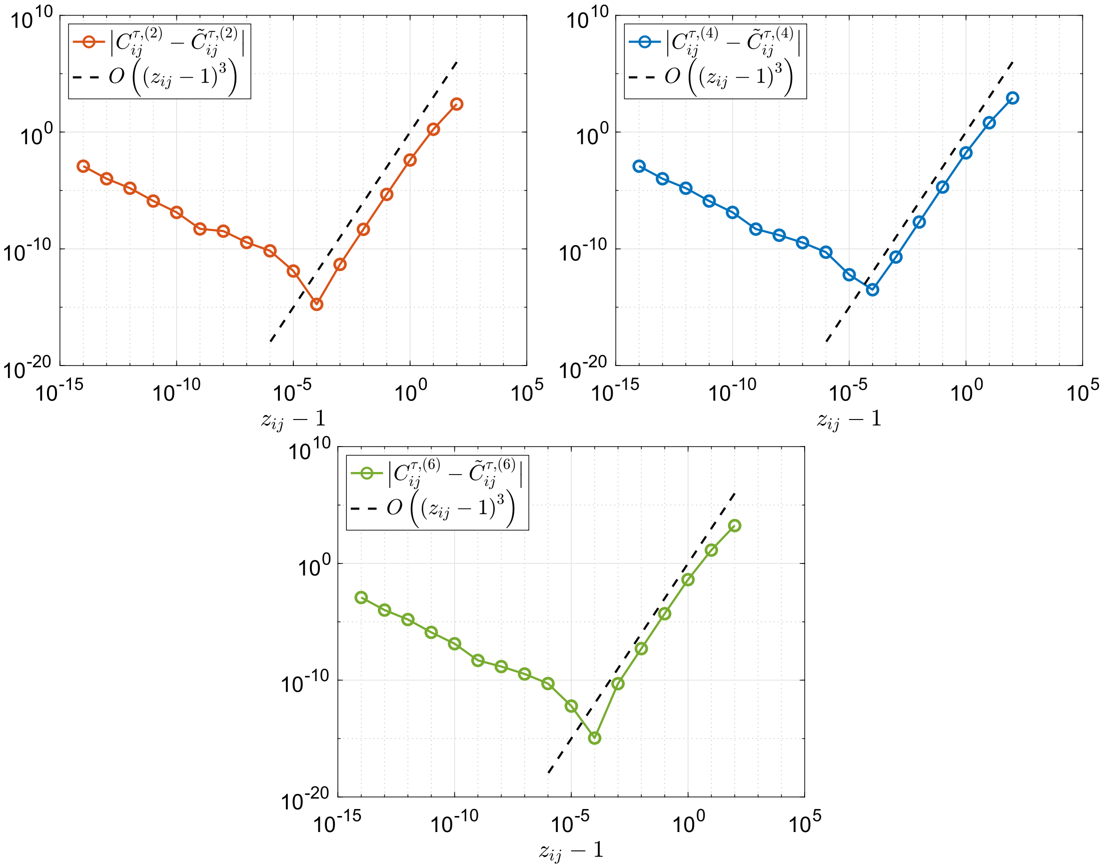

Fig. A.1. Plot of the error between $C_{ij}^{\tau,(m)}$ and its 2nd order Taylor expansion $\tilde{C}_{ij}^{\tau,(m)}$ versus $z_{ij}-1$ for $m=2,4,6$ when $\xi_{ij}^k=1$.

to machine precision when $z_{ij} = \xi_{ij}^{k+1}/\xi_{ij}^k = (r_{ij}^{k+1})^2/(r_{ij}^k)^2$ is close to 1. Furthermore, notice that, after $z_{ij}-1 \approx 10^{-4}$, the error between $C_{ij}^{\tau,(m)}$ and $\tilde{C}_{ij}^{\tau,(m)}$ is almost as small as machine precision for $m=2,4,6$, suggesting that utilizing the Taylor expansions should not lead to loss of accuracy.

References

[1] A.T.S. Wan, A. Bihlo, J.-C. Nave, Conservative integrators for many-body problems, J. Comput. Phys. 466 (2022) 111417, https://doi.org/10.1016/j.jcp.2022.111417.

[2] R.A. Labudde, D. Greenspan, Energy and momentum conserving methods of arbitrary order for the numerical integration of equations of motion, Numer. Math. 26 (1) (1976) 1–16.

[3] J.C. Simo, N. Tarnow, K.K. Wong, Exact energy-momentum conserving algorithms and symplectic schemes for nonlinear dynamics, Comput. Methods Appl. Mech. Eng. 100 (1) (1992) 63–116.

[4] B. Leimkuhler, S. Reich, Simulating Hamiltonian Dynamics, Cambridge Monographs on Applied and Computational Mathematics, Cambridge University Press, 2005.

[5] E. Hairer, C. Lubich, G. Wanner, Geometric Numerical Integration: Structure-Preserving Algorithms for Ordinary Differential Equations, Springer Series in Computational Mathematics, Springer Berlin Heidelberg, 2006.

[6] J.E. Marsden, M. West, Discrete mechanics and variational integrators, Acta Numer. 10 (2001) 357–514.

[7] V. Dorodnitsyn, Applications of Lie Groups to Difference Equations, Differential and Integral Equations and Their Applications, CRC Press, 2010.

[8] P.E. Hydon, Difference Equations by Differential Equation Methods, Cambridge Monographs on Applied and Computational Mathematics, Cambridge University Press, 2014.

[9] P.J. Olver, Geometric foundations of numerical algorithms and symmetry, Appl. Algebra Eng. Commun. Comput. 11 (2001) 417–436.

[10] P. Kim, P. Olver, Geometric integration via multi-space, Regul. Chaotic Dyn. 9 (3) (2004) 213–226.

[11] A. Bihlo, J.-C. Nave, Invariant discretization schemes using evolution-projection techniques, SIGMA 9 (52) (2013) 1–23.

[12] A.T.S. Wan, J.-C. Nave, On the arbitrarily long-term stability of conservative methods, SIAM J. Numer. Anal. 56 (5) (2018) 2751–2775.

[13] J.T. Beale, A. Majda, High order accurate vortex methods with explicit velocity kernels, J. Comput. Phys. 58 (2) (1985) 188–208.

[14] P.K. Newton, The N-Vortex Problem: Analytical Techniques, Springer, New York, 2001.

[15] M. Perlman, On the accuracy of vortex methods, J. Comput. Phys. 59 (2) (1985) 200–223.

[16] O.H. Hald, Convergence of vortex methods for Euler's equations. II, SIAM J. Numer. Anal. 16 (5) (1979) 726–755.

[17] J.T. Beale, A. Majda, Vortex methods. I. Convergence in three dimensions, Math. Comput. 39 (159) (1982) 1–27.

[18] J.T. Beale, A. Majda, Vortex methods. II: higher order accuracy in two and three dimensions, Math. Comput. 39 (159) (1982) 29–52.

[19] P.R. Spalart, Numerical simulation of separated flows, Ph.D. thesis, Stanford Univ., CA, Dec. 1983.

[20] A.Y. Cheer, Numerical study of incompressible slightly viscous flow past blunt bodies and airfoils, SIAM J. Sci. Stat. Comput. 4 (4) (1983) 685–705.
[21] P. Spalart, A. Leonard, Computation of separated flows by a vortex-tracing algorithm, Tech. rep., NASA, 1981.
[22] A. Ghoniem, A. Chorin, A. Oppenheim, Numerical modeling of turbulent combustion in premixed gases, Symp., Int., Combust. 18 (1) (1981) 1375–1383, Eighteenth Symposium (International) on Combustion.
[23] J. Sethian, Turbulent combustion in open and closed vessels, J. Comput. Phys. 54 (3) (1984) 425–456.
[24] A. Leonard, Vortex methods for flow simulation, J. Comput. Phys. 37 (3) (1980) 289–335.
[25] D.D. Holm, H.O. Jacobs, Multipole vortex blobs (MVB): symplectic geometry and dynamics, J. Nonlinear Sci. 27 (2017) 973–1006.
[26] A.T.S. Wan, A. Bihlo, J.-C. Nave, Conservative methods for dynamical systems, SIAM J. Numer. Anal. 55 (5) (2017) 2225–2285.
[27] P.J. Olver, Applications of Lie Groups to Differential Equations, Graduate Texts in Mathematics, vol. 107, Springer-Verlag, New York, 1986.
[28] G.W. Bluman, A.F. Cheviakov, S.C. Anco, Application of Symmetry Methods to Partial Differential Equations, Springer, New York, 2010.
[29] D.D. Holm, M. Nitsche, V. Putkaradze, Euler-alpha and vortex blob regularization of vortex filament and vortex sheet motion, J. Fluid Mech. 555 (2006) 149–176, https://doi.org/10.1017/S0022112006008846.
[30] G. Cottet, P.D. Koumoutsakos, Vortex Methods: Theory and Practice, Cambridge University Press, Cambridge, 2000.
[31] G.K. Batchelor, An Introduction to Fluid Dynamics, Cambridge University Press, Cambridge, 1967.
[32] P.J. Olver, Application of Lie Groups to Differential Equations, Springer, New York, 2000.
[33] W.H. Press, S.A. Teukolsky, W.T. Vetterling, B.P. Flannery, Numerical Recipes in C, Cambridge University Press, Cambridge, 1992.
[34] W.J. Cody, H.C.J. Thacher, Rational Chebyshev approximations for the exponential integral $E_1(x)$, Math. Comput. 22 (103) (1968) 641–649.
[35] A. Ralston, Runge-Kutta methods with minimum error bounds, Math. Comput. 16 (1962) 431–437.
[36] M. Lotkin, On the accuracy of Runge-Kutta's method, Math. Tables Other Aids Comput. 5 (35) (1951) 128–133.
[37] V. Rokhlin, Rapid solution of integral equations of classical potential theory, J. Comput. Phys. 60 (2) (1985) 187–207.
[38] L. Greengard, V. Rokhlin, A fast algorithm for particle simulations, J. Comput. Phys. 73 (2) (1987) 325–348, https://doi.org/10.1016/0021-9991(87)90140-9, https://www.sciencedirect.com/science/article/pii/0021999187901409.